COMPUTER MODELS OF A BASEMENT INVOLVED FAULT PROPAGATION FOLD DURING THE LARAMIDE OROGENY AROUND LAS VEGAS, NEW MEXICO

by

JERRY TIMOTHY FORD

Presented to the Faculty of the Graduate School of

The University of Texas at Arlington in Partial Fulfillment

of the Requirements

for the Degree of

MASTER OF SCIENCE IN ENVIRONMENTAL AND EARTH SCIENCE

THE UNIVERSITY OF TEXAS AT ARLINGTON

May 2015

Dedication

I would like to dedicate this thesis to Christ Jesus, my Lord and Savior, for saving me. Without him I would be eternally separated from him in hell, which I surely do deserve. The love of Jesus is all enduring, and He is the same yesterday, today and tomorrow.

Acknowledgements

Many people have given me their guidance and encouragement throughout this whole process while being unbelievably patient with me, for which I am grateful beyond measure. Countless times, I wanted to just quit and go on with my life, but then someone would nudge me back to reality and get me back to working on completing the task. Without any of these people in my life, I would not have been able to finish my thesis

I would like to thank Dr. John Wickham, Committee Chairman, for offering this project to me. He spent many hours with me troubleshooting and perfecting my FLAC models, especially at the beginning of the project when I knew so little about the program. Many times I would have error codes in FLAC and he would spend his valuable time helping me find the problem. His direction, focus, knowledge, and the editing of my work have been invaluable to me.

Dr. Rich McMullen, thesis committee member, for his expertise in FLAC and engineering so that my project was thoroughly reviewed. He also spent many hours with me determining which areas to investigate further with FLAC. His attention to detail helped me refine my work and see pertinent details that were there all along.

Dr. Arne Winguth, thesis committee member, for spending the time on reviewing this manuscript to polish my written text and his expertise about computer modeling are greatly appreciated.

Brian and Susan Fletcher, personal friends who graciously allowed me to work on their home computer while mine was not working, so that I could create figures from FLAC screenshots and for Susan showing me how to use another software for editing the screenshots to put into my thesis.

Carroll and Prissy Graves, personal friends, who supported me during the whole process.

Most of all, I would like to thank my family, especially my wife Rebecca Ford. Her patience throughout this whole process has exceeded all understanding and she is truly the best wife and friend anyone could hope to have. For all of her support, I am greatly in debt to her. Our two children, Ben and Jessica, also had to endure my time away from them, or endure my wrath for not keeping the noise down. I am very thankful that they have been so forgiving and understanding. To my mom, who never stopped believing that I would finish. I also want to thank Miritha Caperton, my mother-in-law, for taking care of the house and home schooling Ben, so that I could finish my thesis. Her help has been tremendous, especially these last few weeks.

April 20, 2015

Abstract

COMPUTER MODELS OF A BASEMENT INVOLVED FAULT PROPAGATION FOLD DURING THE LARAMIDE OROGENY AROUND LAS VEGAS, NEW MEXICO

Jerry Timothy Ford, M.S.

The University of Texas at Arlington, 2015

Supervising Professor: John S. Wickham

Numerical geomechanical modeling is acceptable today for studying geologic structures and is readily accomplished by most computers used by geoscientists and engineers interested in studying geomechanics. Models should be simple so that too many discontinuities are not introduced. This study creates models of a thrust fault, developed and implemented using the computer program FLAC version 4.0 to simulate the structural evolution of a basement-involved fault propagation fold undergoing shortening and then compares them to a published cross section NW of Las Vegas, New Mexico. FLAC is a numerical 2D modeling program for modeling geologic materials and has large strain capability suitable for this type of study. A Mohr-Coulomb plasticity constitutive rule was used with unequal dilation and friction angles for non-associated plastic flow enabling shear band occurrence.

Folding is developed with approximately a 300 m crest rise, 880 m bed displacement along the associated thrust fault, and with shear bands producing a backthrust zone located near the Medina Syncline location on the published cross section. Void spaces also occur. Although shear bands might be interpreted as faults, FLAC version 4.0 cannot generate new faults, but the produced uplift was similar to the

published cross section and the backthrust creates a surface deformation near to the Medina Syncline. Using the newer version of FLAC version 7.0 could possibly overcome these limitations.

Table of Contents

List of Illustrations

List of Tables

Chapter 1

Introduction

1.1 Geomechanical Models

In the past, numerical geomechanical models were not used routinely in structural geology research, because they could not model the nonlinearities typically encountered in geological problems (Starfield and Cundall, 1988). Advancements in computer technology enables numerical modelers of today to model nonlinearities of geological materials. Also, advances in software have kept abreast with the computer hardware technology, so that the versatile computer programs for modeling geological scenarios have become more robust and enabled the modeler to simulate new or more complicated problems. Geological processes like faulting have numerous complex influences that are difficult to describe and solve mathematically, but geomechanical models can bring about greater understanding, if they are simple geometrically but still model complex physical behaviors. This is something computer modeling can easily accomplish (Harper, 2008; Starfield and Cundall, 1988). Computer modeling can increase our understanding of the basic processes that occur in rock and evaluate the effectiveness of structural and engineering designs (Jing and Hudson, 2002; Jing, 2003; Nino et al., 1998). Within the field of geology, especially structural geology, geoscientists in the mineral and petroleum industry are interested in how faults propagate within basement rock and overlying sediments in order to understand the conditions controlling the deformation. Seismologists and engineers studying the impacts of geological hazards upon humans also consider numerical models quite valuable (Harper, 2008; Jing, 2003; Nino et al., 1998). It should be stressed that there are many possible fault configurations that are acceptable, and that none of the numerical solutions are unique due to the variability of the boundary conditions, loading rates, damping, and mesh size

(Harper, 2008; Gerbault et al., 1998). However, important new information can be gained by carefully constructing numerical models to better understand crustal faulting processes and compare them to field investigations, thereby increasing confidence in their results (Harper, 2008; Jing, 2003; Nino et al., 1998; Starfield and Cundall, 1988).

Considering all of the points mentioned above, this research applies FLAC, a numerical 2D modeling program sold by Itasca Consulting Group. It is used by geoscientists and engineers to model the behavior of geologic materials in mining, petroleum, civil engineering projects, as well as research projects (Coetzee et al., 1995; Itasca Consulting Group, 2002; Starfield and Cundall, 1988; Strayer and Hudleston, 1997). Further details about FLAC basics can be found in the FLAC User's Guide in sections 1-3.

1.2 Other Models and Comparisons

Nino et al., (1998) applied FLAC to study blind thrusting and showed that bed parallel slip causes back thrusts to form, and that the propagation of blind thrusts is mostly influenced by that slippage rather than the different rock rheology. They also studied how fault dip and layer thickness affected fault propagation. Although these models do not allow bed parallel slip between the overburden sediments, there is one slip surface below the sediments and on top of the basement, which acts as a basement fault that produces back thrusts.

FLAC models have also been used to study faulting during extensional and shortening processes through crystalline basement and overlying sediments, which produced structures similar to field observations, but the author concluded additional work was needed (Harper, 2008). The models used in this study are similar in size to the (Harper, 2008) models, but this project only uses compression.

In another similar study, FLAC was used to investigate a smaller model of an extensional fault propagation fold (Cardozo and Cuisiat, 2008). Their model used a finer mesh and smaller overall size than the one in this study but they also used remeshing in order to compensate for the large deformations formed at the fault tip.

In yet another study, FLAC was used to model various geologic structures during the initial development of folds along thrust ramps (Strayer and Hudleston, 1997). They studied four different models including fault propagation folds (paired and singular with no through-going faults), fault bend folds, and wedge folds with a through-going fault. Even though their models were only meter scale versus kilometer scale as in this model, they were able to model folds similar to examples found in outcrop settings. Their model B is the most similar to the models in this study, since it simulates a fault propagation fold.

Another similarity between the (Strayer and Hudleston, 1997) models and the models in this study is the occurrence of voids along the fault interface; additional comparisons are discussed in section 4.2. These voids were described as “areas of low pressure” where minerals such as quartz and calcite have filled the void spaces (Strayer and Hudleston, 1997). The voids may disappear if timing of thrusting versus model time was more accurate. As in this study, large mesh distortions occurred at the fault tips causing FLAC to stop due to “an ‘invalid geometry’ error” (Cardozo and Cuisiat, 2008). All of the simulations in this study produced backthrust shear bands of deformation. Other studies have also produced backthrust shear bands in fault bend folding models by (Erickson et al., 2001); and especially in the fault propagation fold models by (Nino et al., 1998; Strayer and Hudleston, 1997).

Chapter 2

Geologic Study Area

2.1 Location and Description

The study area is near the town of Montezuma, New Mexico, and is located approximately 5 miles north of Las Vegas, New Mexico on New Mexico highway 65, in the southern range of the Sangre de Cristo Mountains of north-central New Mexico, see Figure 2.1. This area is typical of basement involved foreland block uplifts, and has numerous exposures of faults, slicken lines, and joints from which data can be collected and evaluated, making this area quite suitable for rock deformation studies of the "Laramide-age" (80 to 55 Ma). A large fault, the Montezuma Fault, separates the Sangre de Cristo Mountains from the great plains and is a very prominent linear feature on satellite images. The Montezuma Fault outcrops on the eastern half of the United World College campus and trends linearly in a north-south direction.

2.2 Data Collected

A hot spring near the town of Montezuma suggests that a fault could be present supplying the water for the springs, especially since the main anticline and Montezuma Fault found to the west of Las Vegas is located less than one quarter of a mile away from the hot springs. Strike and dip measurements were collected along a transect perpendicular to the Montezuma Fault parallel to New Mexico highway 65 as well as mapping conducted during May and June of 2008 and 2009. Additional data comes from the USGS geological map of the Gallinas Creek Area (Baltz, 1972).

2.3 Cross-Section Model and Published Section Comparison

A model was created to simulate the deformation of a fault propagation fold similar to that shown in the partial cross section F-F' (Figure 2.2) and from the USGS quadrangle map of the Gallinas Creek Area (Baltz, 1972) (Figure 2.3). To simplify the

model, detailed stratigraphy, minor faults, and erosion were not included (Itasca Consulting Group, 2002; Starfield and Cundall, 1988; Strayer and Hudleston, 1997). Strata are discussed in more detail in section 3.3. Other minor faults are simulated by localized bands of deformation in the FLAC model, but the model geometry only contains one fault interface and it originates in the basement similar to the cross section by Baltz (1972) (Figure 2.3).

Figure 2.1: Location of study area and inset showing global view (Nationalatlas.gov, NM reference map)

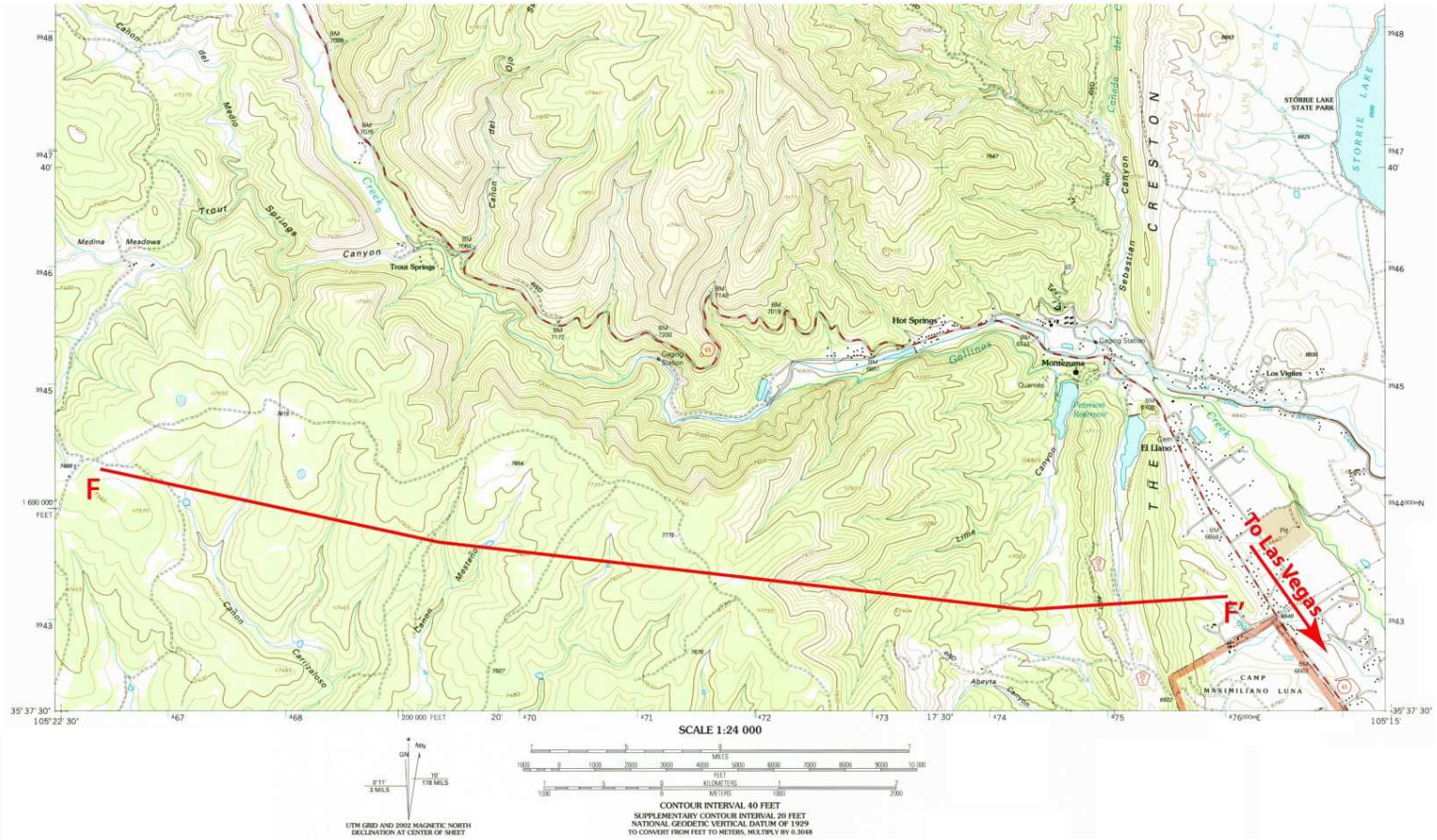

Figure 2.2: Topographical map of study area showing section F-F', near Gallinas Creek at Las Vegas, NM (USGS, Montezuma NM, 2002).

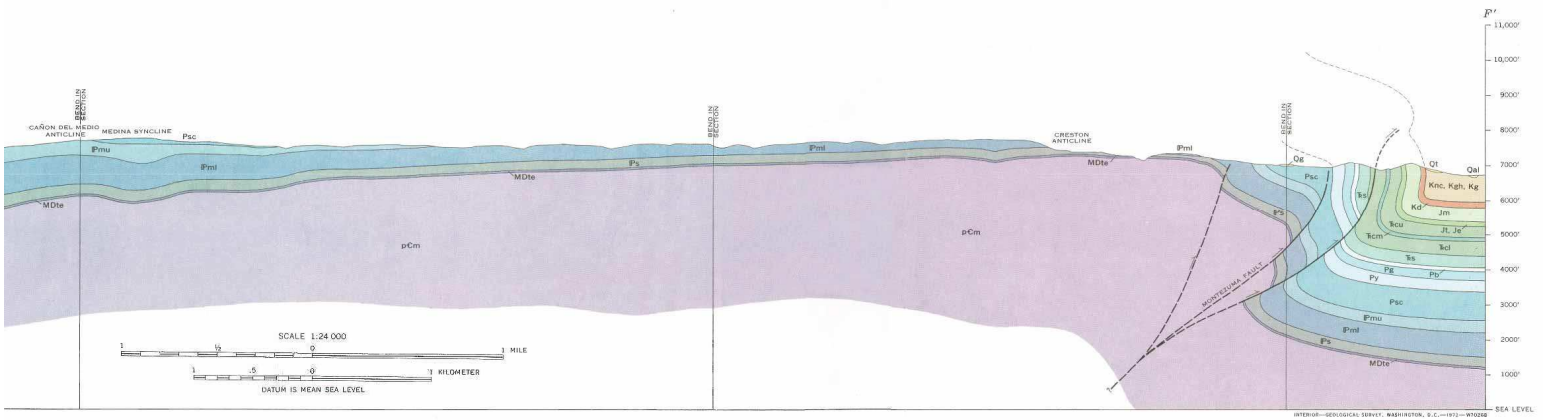

Figure 2.3: Cross Section F-F', near Gallinas Creek at Las Vegas, NM (see Figure 2.2) (Baltz 1972).

Chapter 3

Methodology

3.1 FLAC Description

FLAC (Fast Lagrangian Analysis of Continua) “is an explicit, finite difference” code for two dimensional modeling of the behavior of geologic materials and other materials (Coetzee et al., 1995; Itasca Consulting Group, 2002). When a material reaches its’ yield limit, plastic flow can occur, and geoscientists and engineers in mining, petroleum, civil engineering, as well as research projects and glacial studies are interested in simulating this behavior (Itasca Consulting Group, 2002; Jing, 2003). FLAC can be fine-tuned to model any type of material or shape made up of zones or elements (Coetzee et al., 1995; Itasca Consulting Group, 2002). FLAC3D is the three dimensional version for more detailed simulations and was not used in this study (Itasca Consulting Group, 2002). Since the geomechanical behavior is very complicated, it would not be helpful to make the model more complex (Itasca Consulting Group, 2002; Starfield and Cundall, 1988). FLAC has been used in this study to model large, plain strain deformation of a fault propagation fold, and by others to model other geologic structures (Cardozo and Cuisiat, 2008; Coetzee et al., 1995; Erickson et al., 2001; Itasca Consulting Group, 2002). The main advantage FLAC has over finite-element methods is the use of explicit formulation, so that matrices are not required during each “timestep”, thereby increasing computational speed and making it well matched for nonlinear materials (Coetzee et al., 1995; Erickson et al., 2001; Itasca Consulting Group, 2002; Jing and Hudson, 2002; Jing, 2003). Each grid point or node is numerically related to its’ closest surrounding nodes (Erickson et al., 2001) and in order to reach equilibrium, algebraic equations of the unknowns at those grid points must have small timesteps to keep errors

low (Coetzee et al., 1995; Jing, 2003; Jing and Hudson, 2002; Itasca Consulting Group, 2002).

FLAC solves for any "new velocities and displacements from known stresses and forces" by applying the equations of motion (equilibrium equation), and then uses those velocities to compute new strain rates, and finally uses the new strain rates to obtain new stresses (constitutive equations). This is a looping cycle and is defined as "one timestep", but "the velocities are assumed to be frozen" for one cycle of the loop. Since the timestep is assumed to be infinitesimal, it takes a few timesteps for displacements to affect surrounding elements. The infinitesimal timestep can be a disadvantage, because it requires great numbers of timesteps to produce finite deformation. This effect is exaggerated the most whenever models contain large numbers of elements or zones, due to the computation time needed to cycle through the required timesteps for each element (Coetzee et al., 1995; Itasca Consulting Group, 2002). Models need to be optimized to reduce this effect and improve overall efficiency, as discussed later at the end of section 3.2.

One author states that the system of grid points is, "an approximation of a continuous system with infinite degrees of freedom by a discrete system with finite degrees of freedom" (Jing, 2003). FLAC is particularly useful for thrust fault modeling as the software has large strain capability, is non-linear, and has plasticity models suitable for soil and rock. In FLAC, "the material can yield and flow, and the grid can deform in large-strain mode and move with the material that is represented" (Coetzee et al., 1995; Itasca Consulting Group, 2002).

The relationship between acceleration, $d\dot{\mu}/dt$, a mass, *m*, to an applied force, *F*, defines Newton's law of motion as:

$$m\frac{d\dot{u}}{dt} = F \quad (1)$$

"In a continuous solid body, *Eq.* (1) is generalized as follows:"

$$\rho\frac{\partial \dot{u}_i}{\partial t} = \frac{\partial \sigma_{ij}}{\partial x_j} + \rho g_i \quad (2)$$

where ρ = mass density;

t = time*;*

x_i = components of coordinate vector;

g_i = components of gravitational acceleration (body forces); and

σ_{ij} = components of stress vector.

"Indices *i* denote components in a Cartesian coordinate frame, and summation is implied for repeated indices in an expression" (Itasca Consulting Group, 2002).

3.2 Material Mechanical Behavior

FLAC version 4.0 has ten constitutive models available to use, which are grouped into: null, elastic, and plastic. The Mohr-Coulomb plasticity constitutive rule was chosen to simulate the mechanical behavior of the stratigraphy and the brittle rock failure of the upper crustal rocks in this study (Erickson et al., 2001; Gerbault et al., 1998; Smart et al., 2009; Strayer and Hudleston, 1997). The plastic flow rule and a yield function make up the plasticity rule (Poliakov and Herrmann, 1994). The beginning of plastic behavior is controlled by the yield function *f*, which is:

$$f = \tau + \sigma \sin\phi - C\cos\phi \quad (3)$$

where τ is the shear strength, σ is the mean stress, ϕ is internal friction (a function of strain), and *C* is the cohesion (Cardozo and Cuisiat, 2008; Erickson et al., 2001; Itasca Consulting Group, 2002; Vermeer and de Borst, 1984). The plastic flow is controlled by the plastic potential function *g*, which is:

$$g = \tau + \sigma \sin \psi - C \cos \psi \quad (4)$$

where ψ is the dilation angle, (Cardozo and Cuisiat, 2008; Erickson et al., 2001; Vermeer and de Borst, 1984) the ratio of plastic volume change over plastic shear strain (Itasca Consulting Group, 2002; Poliakov and Herrmann, 1994; Vermeer and de Borst, 1984). The dilation angle is a measure of the shear dilatancy, or just dilatancy, and is the increase in volume of a material (like rock) during shear (Itasca Consulting Group, 2002; Poliakov and Herrmann, 1994; Vermeer and de Borst, 1984).

Non-associated plastic flow is achieved whenever the dilation angle and friction angle are not equal (Erickson et al., 2001; Poliakov and Herrmann, 1994; Strayer and Hudleston, 1997; Vermeer and de Borst, 1984). Localized plastic deformation can occur in FLAC whenever a non-associated plastic flow rule is used (Gerbault et al., 1998; Strayer and Hudleston, 1997), and it is also grid size dependent (Cardozo and Cuisiat, 2008; Erickson et al., 2001; Strayer and Hudleston, 1997). Using FLAC to simulate pure shear, Poliakov and Hermann (1994), showed that the localized shear bands formed fractal networks and that their length distribution resulted in a self-organized criticality. Non-associated plasticity localizes material deformation depicted by plastic shear zones surrounded by elastic elements (Gerbault et al., 1998). The equations of motion in FLAC enables shear band localization to occur (Erickson et al., 2001; Strayer and Hudleston, 1997), which then dissipates the kinetic energy (Erickson et al., 2001; Itasca Consulting Group, 2002; Strayer and Hudleston, 1997). No discontinuities are introduced into the model due to the shear bands so that all regions remain continuous except for interfaces, which are used to model the major thrust fault interface before the simulation (Erickson et al., 2001; Strayer and Hudleston, 1997).

A problem with shear bands is that their thickness is controlled by the size of the elements (Erickson et al., 2001; Gerbault et al., 1998; Poliakov and Herrmann, 1994;

Strayer and Hudleston, 1997). As a mesh becomes finer, or more elements per area, shear bands become thinner. Since shear bands are dependent upon the size of the element and natural rocks tend to have small grain sizes, modeling of natural rocks is limited to a finer mesh (Poliakov and Herrmann, 1994). In order to optimize shear band localization, numerous less complex simulations were made to locate the shear bands, so that those specific areas could have a finer mesh than the rest of the model. Some areas had very little deformation, so a larger mesh size was used in those areas, thereby improving the overall model efficiency (Itasca Consulting Group, 2002).

3.3 Mesh Creation

Selecting the appropriate material properties for numerical modeling of large scale geologic structures can be difficult due to the lack of data for those larger systems. Laboratory specimens can differ from larger rock systems, because large scale rock masses cannot be considered to be homogeneous, continuous, or isotropic (Strayer and Hudleston, 1997). Due to those uncertainties, a generic approach was chosen for the strata in the model, which simplified the work. It is critical for numerical rock modeling to be more simplified, because models can be overwhelmed by the complexities of too much detail (Starfield and Cundall, 1988; Strayer and Hudleston, 1997). An approximation of the stratigraphy was used by grouping the similar rock types together and taking a weighted average of their material properties. The material properties for the model are shown in Table 3.1. As discussed earlier in section 3.2, the model meets the criteria of non-associated plasticity since we use a dilation angle $\psi = 0^{\circ}$ and the internal friction angle ϕ varies with the rock type. An interface is built into the model, which can be 'glued' or 'unglued' to control whether slip occurs along the surface; it represents a fault or bedding surface with properties consisting of: coefficient of sliding friction, normal stiffness, and shear stiffness.

The simulation is a 2D plane strain model of a fault propagation fold with elastic-plastic material properties for the hanging wall and elastic properties for the footwall. The initial configuration of the model is shown in Figure 3.1; it is 21.6 km long and 3.3 km deep. There are 46,308 elements in each model (Figure 3.1) with the vast majority located within region A (35,000) and region B (7,875). Regions C, D, E, and F are comprised of: 225, 1,472, 1,196, and 540 elements respectively. Regions A and B are element 'rich' with a finer mesh due to the large deformation that occurs in those two areas. The element size for region A measures 20 m on each side, B is 40 x 20m, C is 200 x 100 m, D & E are both 100 m on each side, and F is 200 m on each side.

In order to account for the overburden that was present during the Laramide orogeny, the stratigraphic thickness of the eroded pre-Larimide sediments was estimated from Baltz (1972), (Figure 3.2). The eroded overburden estimate resulted in 18 MPa of pressure on the rocks now exposed at the surface. This pressure and gravity loading were applied to each element across the top surface to simulate the overburden. No other erosion or deposition was taken into account by the model.

The model was designed to simulate the overall geology of the region where the stratigraphy is above a simulated granitic basement (Figure 3.2). The initial fault is in the basement with a flat and ramp geometry. The ramp ends at the basement sediment interface. The fault ramp was designed to be 900 m high with a 24.2º dip and a frictionless interface (μ = 0).

Table 3.1: Material properties (Itasca Consulting Group, 2002; Whittaker et al., 1992)

		Mohr-Coulomb					
		Elastic Properties		Plastic Properties			
Rock	Density (kg/m^3)	Bulk (Pa)	Shear (Pa)	Cohesion (C) (Pa)	Tension (Pa)	Friction angle (ϕ)	Dilation angle (ψ)
Dakota, Entrada, Morrison	2600	2.68055532E+10	6.99275370E+09	2.72E+07	1.17E+06	27.8°	0°
Chinle, Santa Rosa, Bernal	2500	8.80952420E+09	4.30232580E+09	3.84E+07	1.44E+07	14.4°	0°
Glorieta, Yeso	2600	2.0000E+10	8.8900E+09	3.00E+07	2.08E+06	30°	0°
Sangre de Cristo, Alamitos	2533	1.4806E+10	5.1990E+09	3.47E+07	1.00E+07	21°	0°
Porvenir, Sandia, Mississippian	2650	1.9410E+10	7.4480E+09	2.41E+07	5.72E+06	27°	0°
Granite	2700	4.39285680E+10	3.02459003E+10	5.51E+07	1.17E+07	51°	0°

Interface Properties					
Fault Type	Normal Stiffness (Pa/m)	Shear Stiffness (Pa/m)	Cohesion (C) (Pa)	Friction angle (ϕ)	Dilation angle (ψ)
Fault Flat	1.0000E+10	1.0000E+10	23,000	0°	0°
Fault Ramp	1.0000E+10	1.0000E+10	23,000	0°	0°

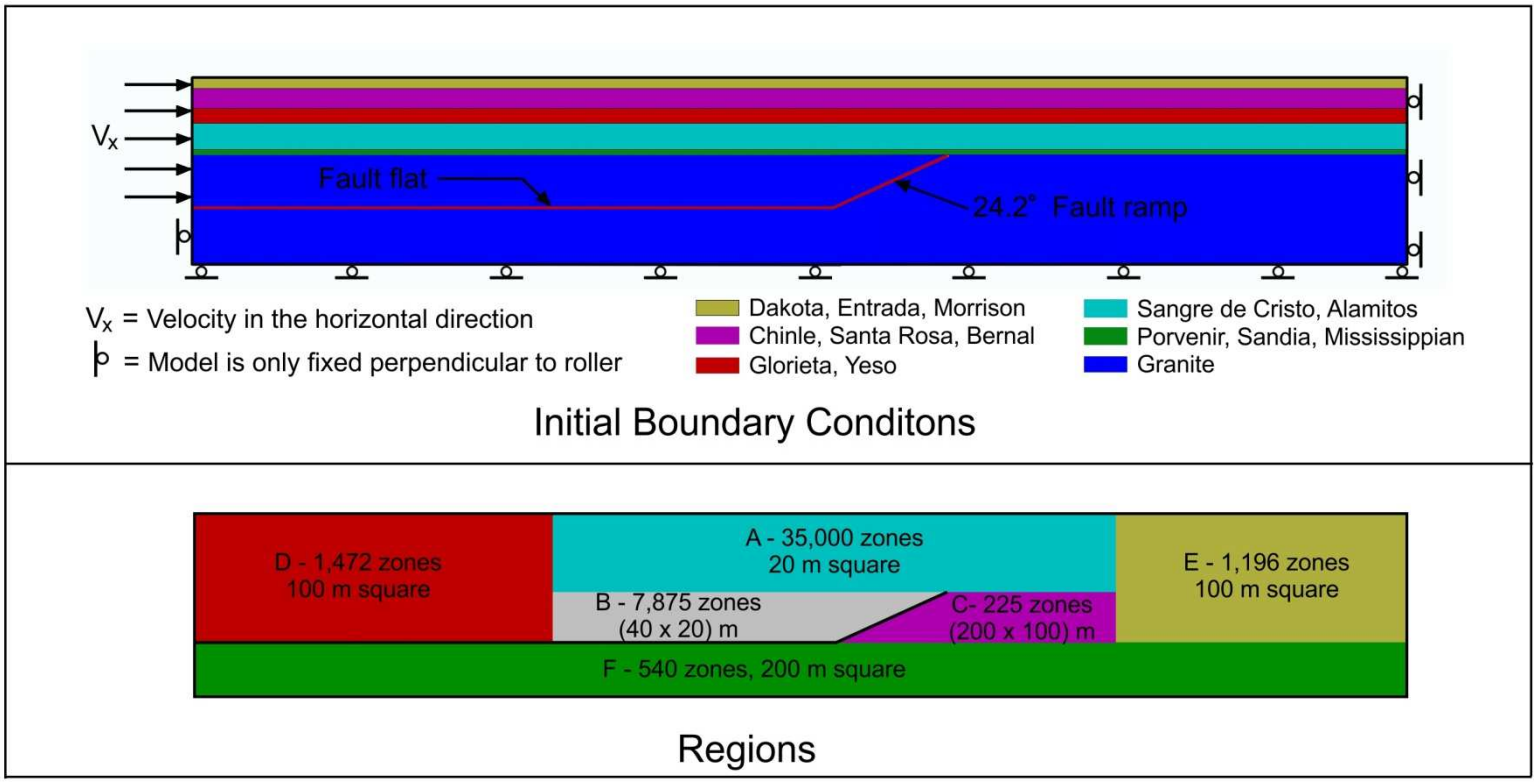

Figure 3.1: Initial boundary conditions are shown in the top figure and the respective regions below.

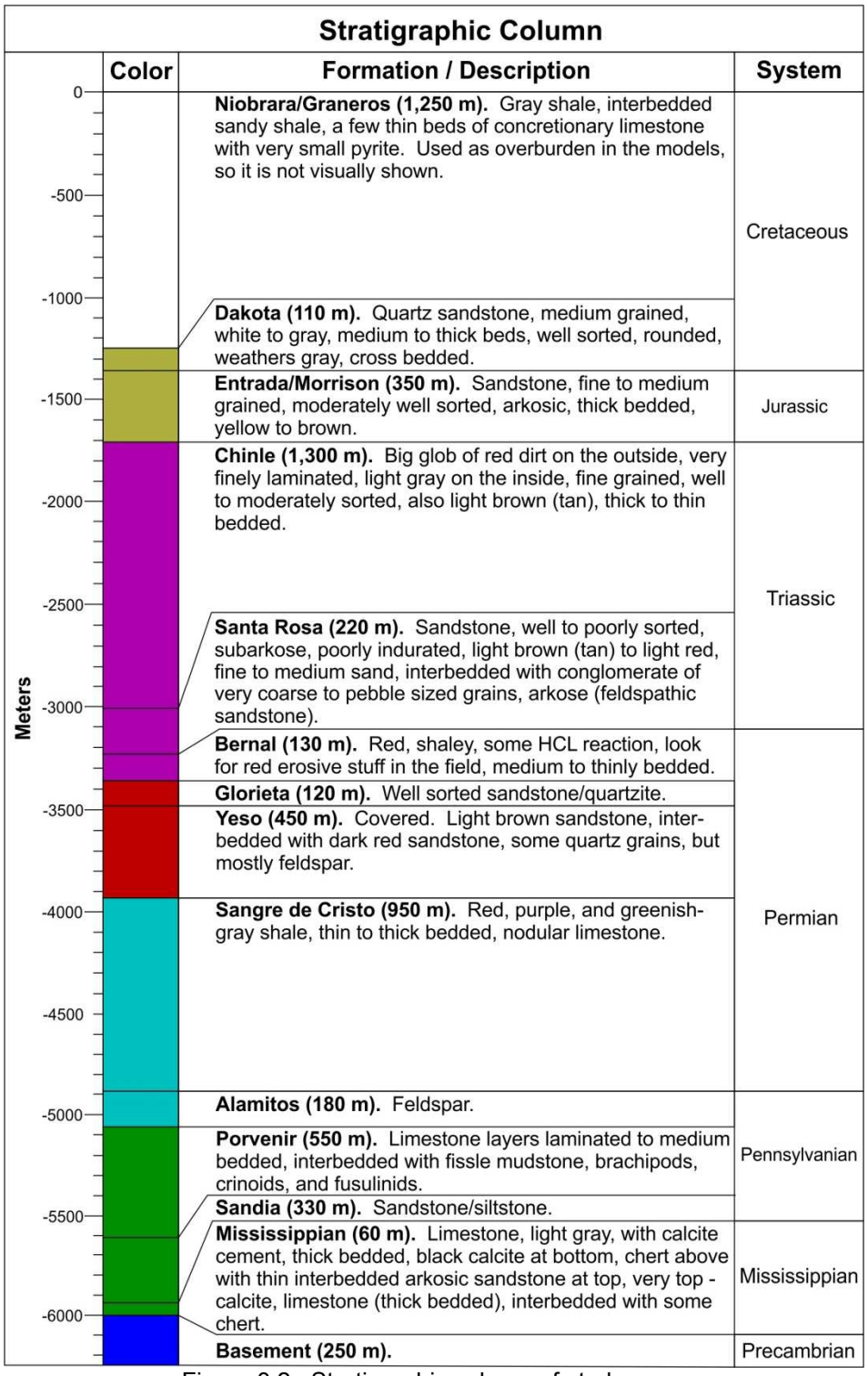

Figure 3.2: Stratigraphic column of study area.

Modeling is accomplished in two stages: stage one is an equilibration step to get the model to an initial state of stress; stage two applies the velocities necessary to produce fault propagation folding. In stage one, displacement can occur parallel to the fixed boundaries but not perpendicular to them, and gravity is applied to each element. The estimated overburden stress is applied to the top of the model. To equilibrate the model, the constitutive equation for the grid elements are temporarily chosen to be elastic, while the fault interface built into the model is temporarily 'glued' to prevent sliding (Cardozo and Cuisiat, 2008). The 'solve' command is used for equilibration and FLAC will stop the program to let the user know when equilibrium has been reached. After the model reaches equilibrium, the material properties are changed to those listed in Table 3.1, and the fault interface is allowed to slide by selecting the 'unbounded' parameter under interface properties using normal and shear stiffness values from Table 3.1. The strata, which is above the fault on the left end of the model (Figure 3.1), is unbound by removing the roller condition and then applying a velocity of 0.02 m/s along that respective boundary. Since there was no evidence of slickensides between beds observed in the field, bed parallel slip was not allowed between the beds.

Each simulation has to be stopped before the geometry of some elements becomes too distorted for reliable calculations, the grid is remeshed to make the distorted elements more symmetrical. The number of times a typical model was remeshed ranged from five to twelve times. The simulation then continues until the elements again become too distorted. The process is repeated until the simulation will not continue any further or it is similar to the structure in the field. This approximates the geologic process being studied and is considered a solution.

The final model configuration was developed by conducting numerous smaller and simpler models to refine it to the point shown in Figure 3.3. Overall, seventy-one

models were created. Thirteen models were chosen to represent the progression of models from simple to the more complex model used in this study. These thirteen are included for reference in Appendix B. Appendix A is a table listing the parameters of each model listed in Appendix B. Three complete models of the final geometry were run (Figure 3.4) and the model with the greatest displacement and number of steps was used for final evaluation (Figure 3.4, Model 14). The last three models contain the same model parameters, but all of the earlier models are simpler in construction. The earlier models were constructed to determine the best mesh size and locate the finer mesh in the middle area where shear band propagation was occurring as a back thrust. Once the simple models behaved consistently, additional parameters were added to more closely approximate the stratigraphy, while comparing the new results with the earlier and simpler models. Also, another model was constructed to calibrate a similar study of a fault bend fold (Erickson et al., 2001), to study firsthand how FLAC handled the hanging wall rock moving and deforming over a footwall. Duplicating their work also helped to refine the model boundary conditions and test modeling skills. Duplication of their work was not included in the appendix.

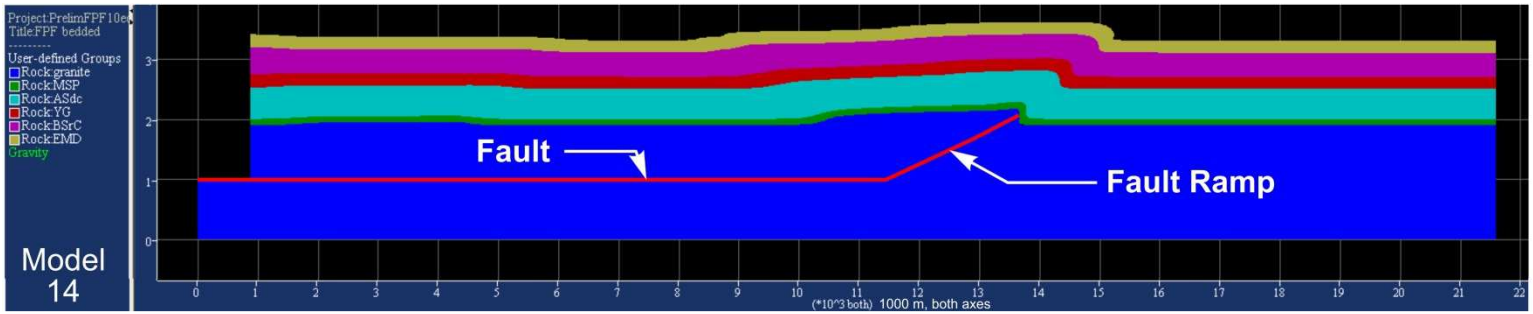

Figure 3.3: Final model configuration. Scale of axes – 1 km.

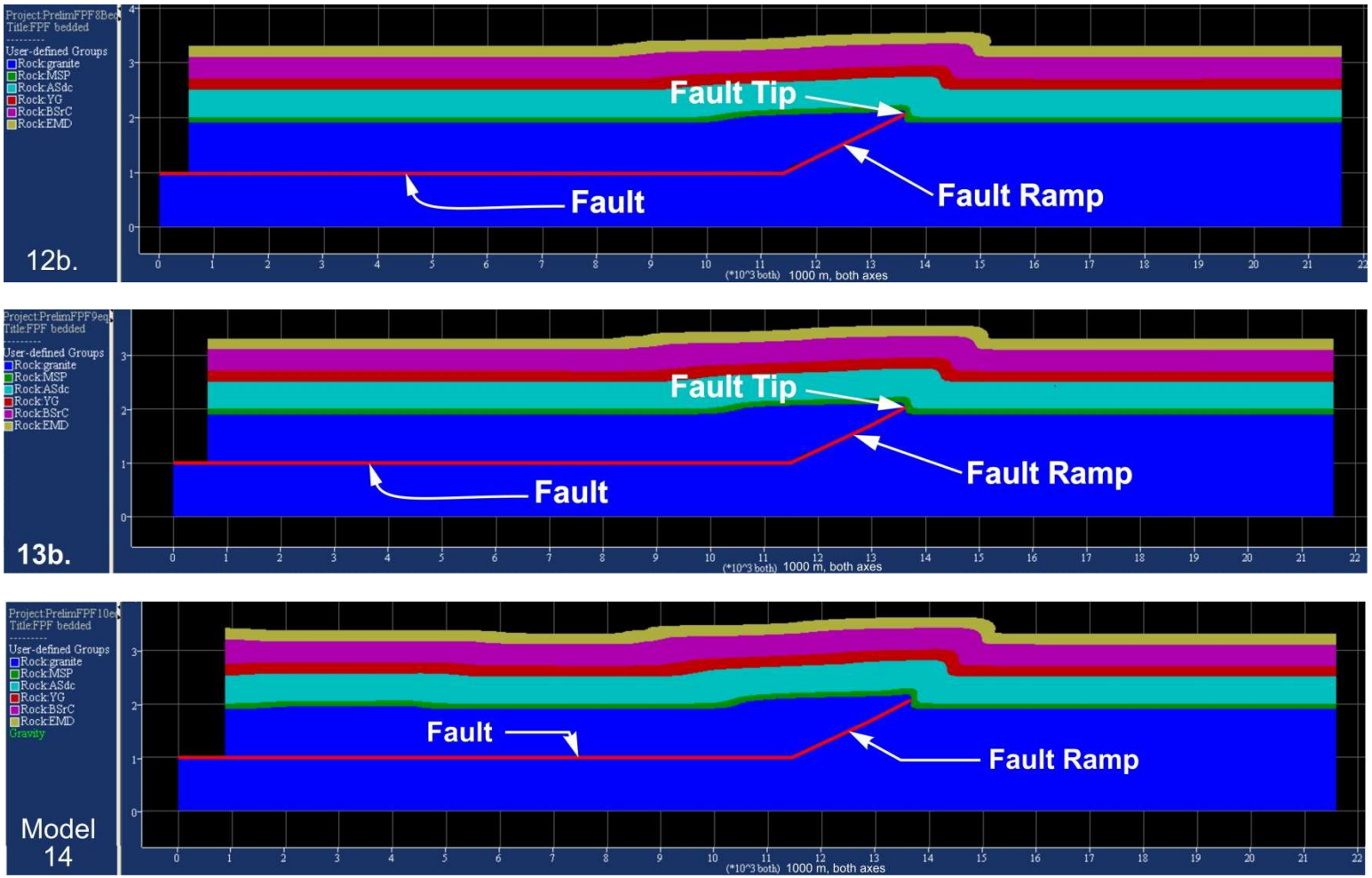

Figure 3.4: Comparisons of final three models, each at final configurations. Scale of axes – 1 km.

Chapter 4

Results

4.1 Propagation of Basement Fault into the Sediments

As expected, the fault tip propagated in the direction of the basement ramp angle, but instead of the fault growing by cutting into the sediments, it displaced the sediments in the direction of fault travel, forming an asymmetric fault propagation fold (Figure 4.1). Some thickening of the beds occurs along the axial surface of the folds. Another feature of the deformation was the deformation/elongation of the mesh elements in the footwall at the fault tip (Figure 4.2). This is a ductile behavior, and a possible explanation of the elongation of these elements would be the buildup of fault gouge and fault breccia in this region. The whole area surrounding the tip-fold zone exhibits ductile behavior, and this is characteristic of the ductile zones found around fault tips in thrust faults.

4.2 Fault Propagation Fold Development

The fault tip has a throw of 150 meters and a heave of 300 meters to the right (Figure 4.2). There are shear bands beginning at the fault tip and ending at the surface near the steep forelimb dip (Figure 4.3). There are shear bands indicating tension failure near the surface of the forelimb and extending a short distance back where tension cracks would be expected in outcrop. Below the fault propagation fold, there are shear bands suggesting an antithetic and a synthetic fault. At the surface, the forelimb dip of the fold is approximately 90º and the crest of the fold is approximately 300 meters higher than the trough, while near the fault tip, the dip of the bottom bed contact is slightly less than 90º (Figure 4.1 and Figure 4.2). Fault displacement on the left hand end of the model equals 880 meters (Figure 4.4).

In all models, void spaces would form along the interfaces at the beginning of the

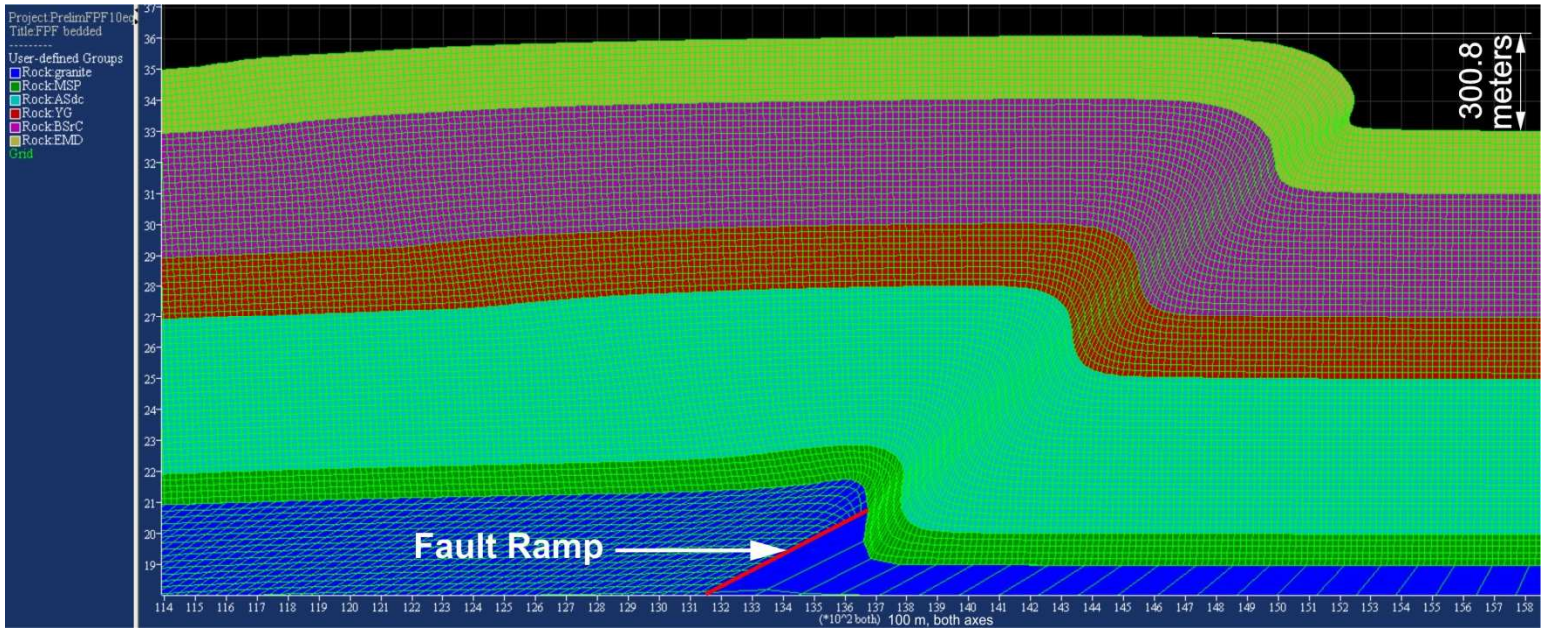

Figure 4.1: Folding at fault ramp. Scale of axes – 100 m.

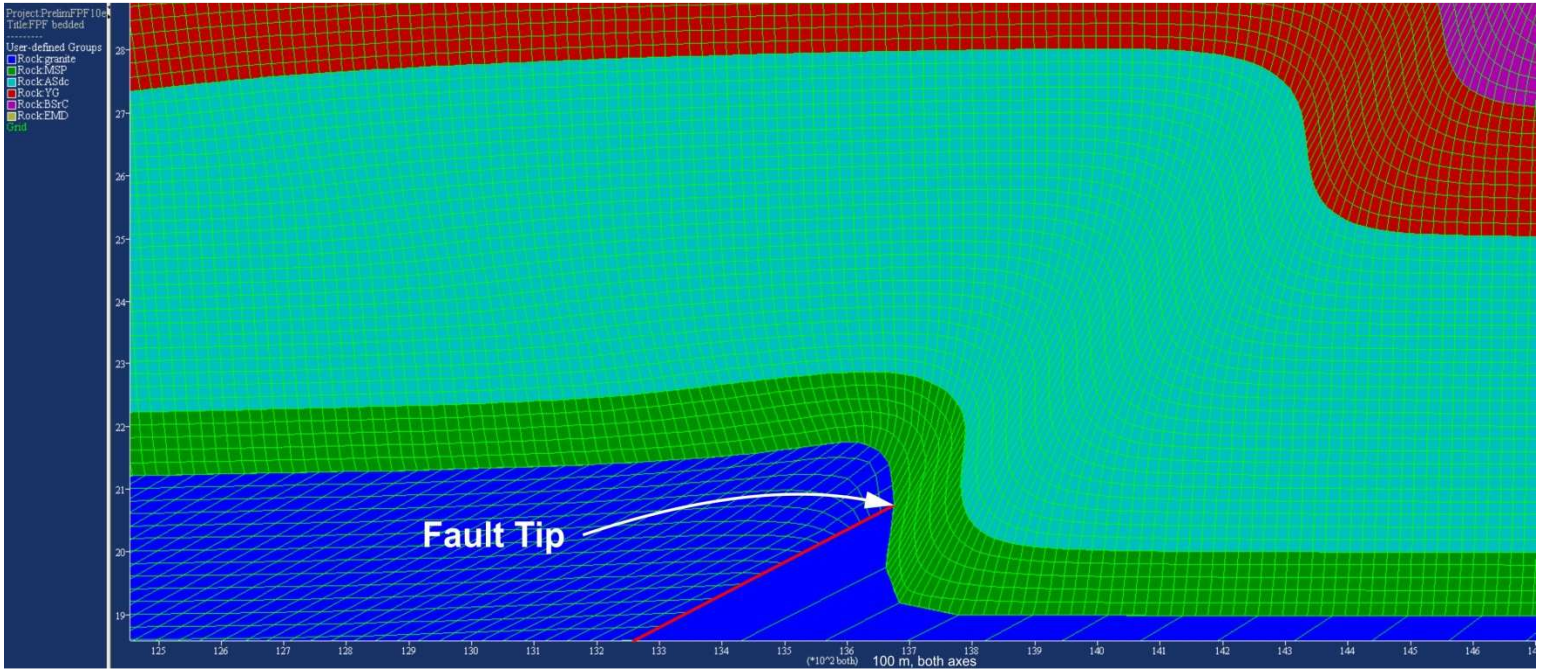

Figure 4.2: Fault tip close up. Scale of axes – 100 m.

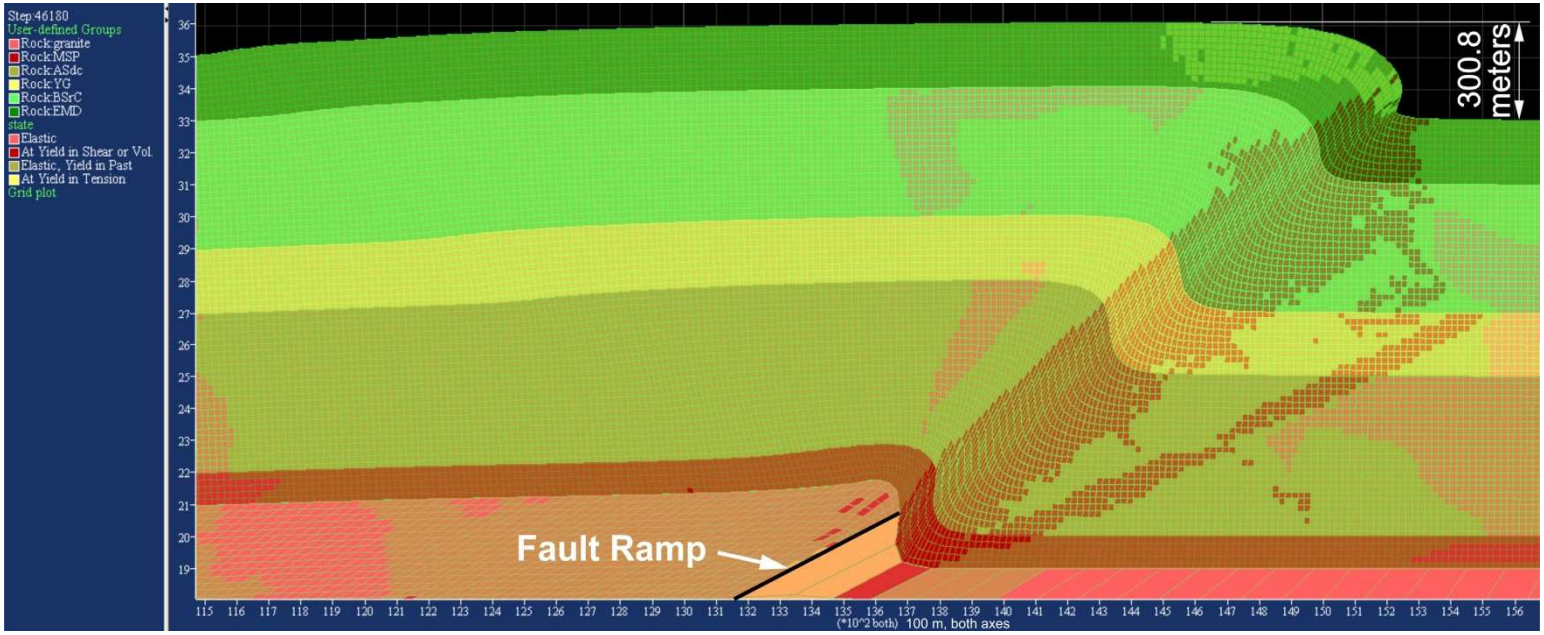

Figure 4.3: Shear bands at fault tip. Scale of axes – 100 m.

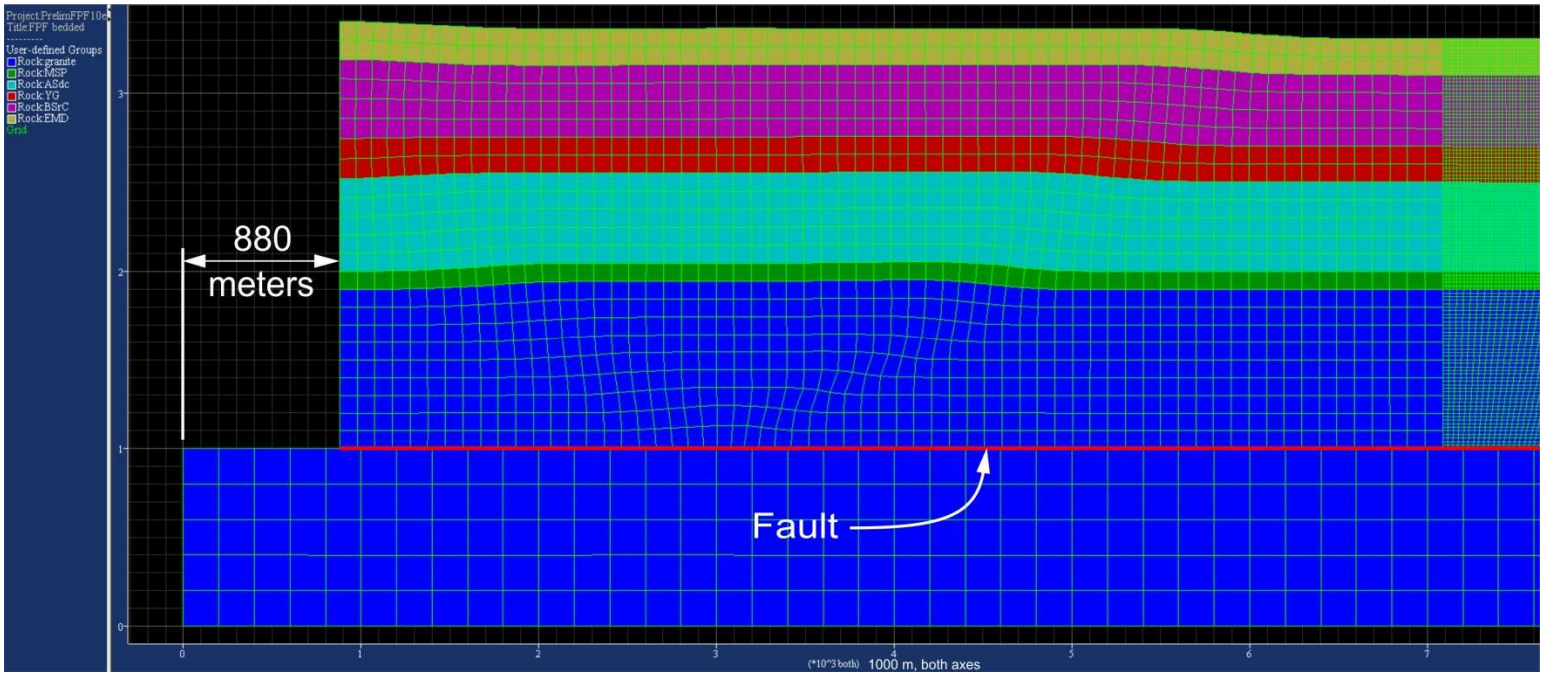

Figure 4.4: Left hand end of model, final position. Scale of axes – 1 km.

fault ramp (Figure 4.5). These spaces are an indication of low pressure zones or errors in timing of thrust development, fault geometry, or material properties, and natural field examples could be infillings of quartz or calcite (Strayer and Hudleston, 1997).

4.3 Medina Syncline, Backthrusting and the Fault Bend

The Medina Syncline can be found on the Baltz (1972) cross section near the left hand end (Figure 2.3). A similar compressional geological folding structure occurs at approximately the same distance from the main fault in each of the models (Figure 4.6). Early into each simulation, a zone of plastic failure similar to a backthrust, would begin at the fault bend in the basement and propagate to the surface near the location of the Medina Syncline on the (Baltz, 1972) cross section. The zone of plastic failure in this area is actually comprised of an upper and lower zone, with the lower zone containing slightly wider bands of failure. The failure zones are similar to a backthrust dipping opposite to the major fault. Also, plastic failure bands are much wider near the bend of the fault ramp, which is within the granite basement, but they become narrower above the granite within the sedimentary beds. In the earlier models, the patterns were attributed to the differences of grid size and shape between the basement (granitic) material and the overlying sediments (Figure 4.7); but additional models suggested that the major controlling factor was not the grid pattern or grid shape, but instead the rock rheology that the shear bands were propagating through. This conclusion can be verified by comparing the shear band patterns of models with only one rock rheology above the fault surface to models with multiple rock rheologies above the fault surface (Figure 4.8, Figure 4.9, Figure 4.10, and Figure 4.11). Further models need to be constructed to verify this conclusion.

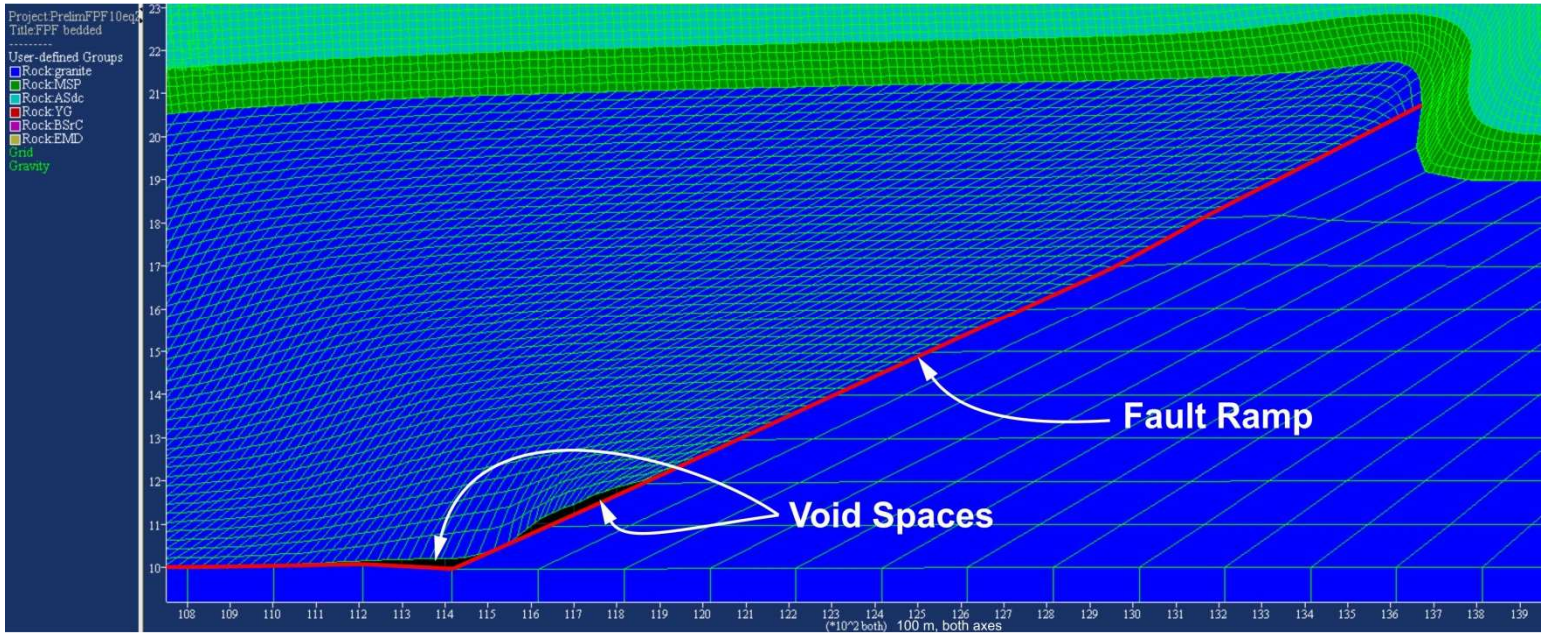

Figure 4.5: Void space formation at fault bend. Scale of axes – 100 m.

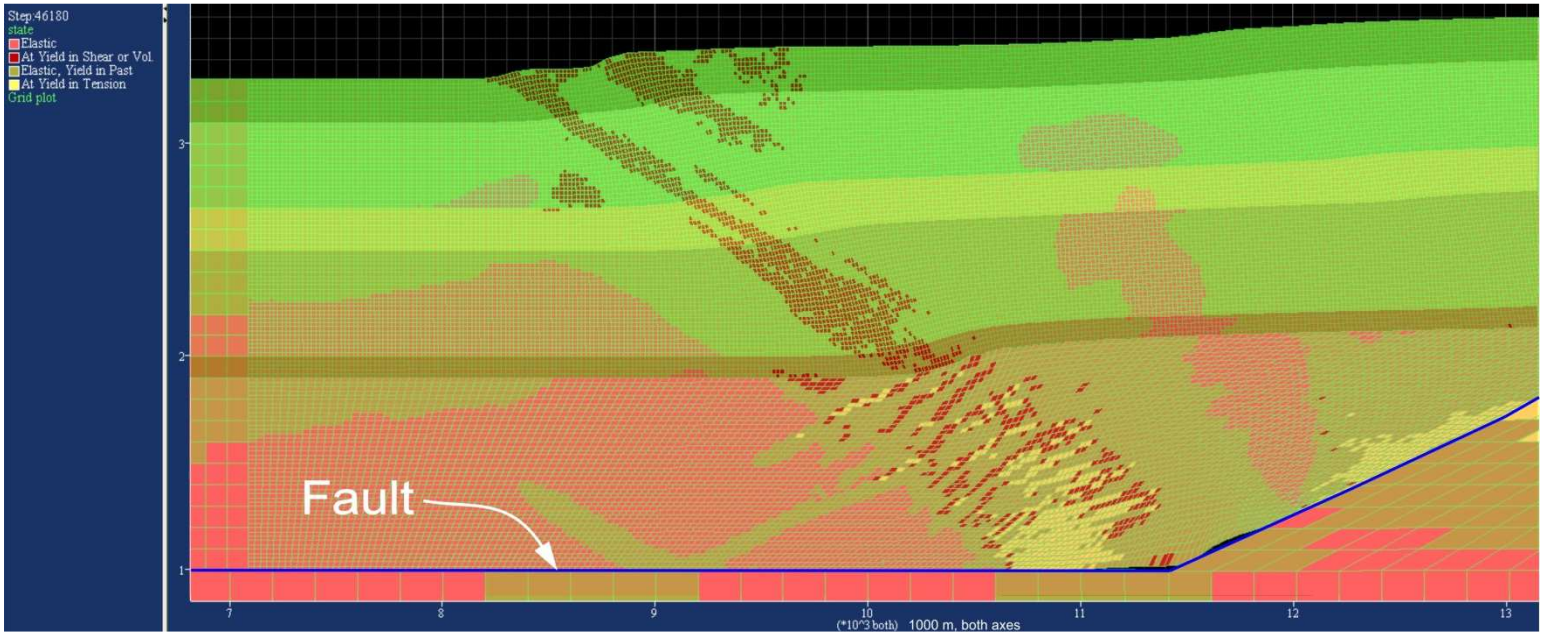

Figure 4.6: Backthrust and shear bands originating from fault bend. Scale of axes – 1 km.

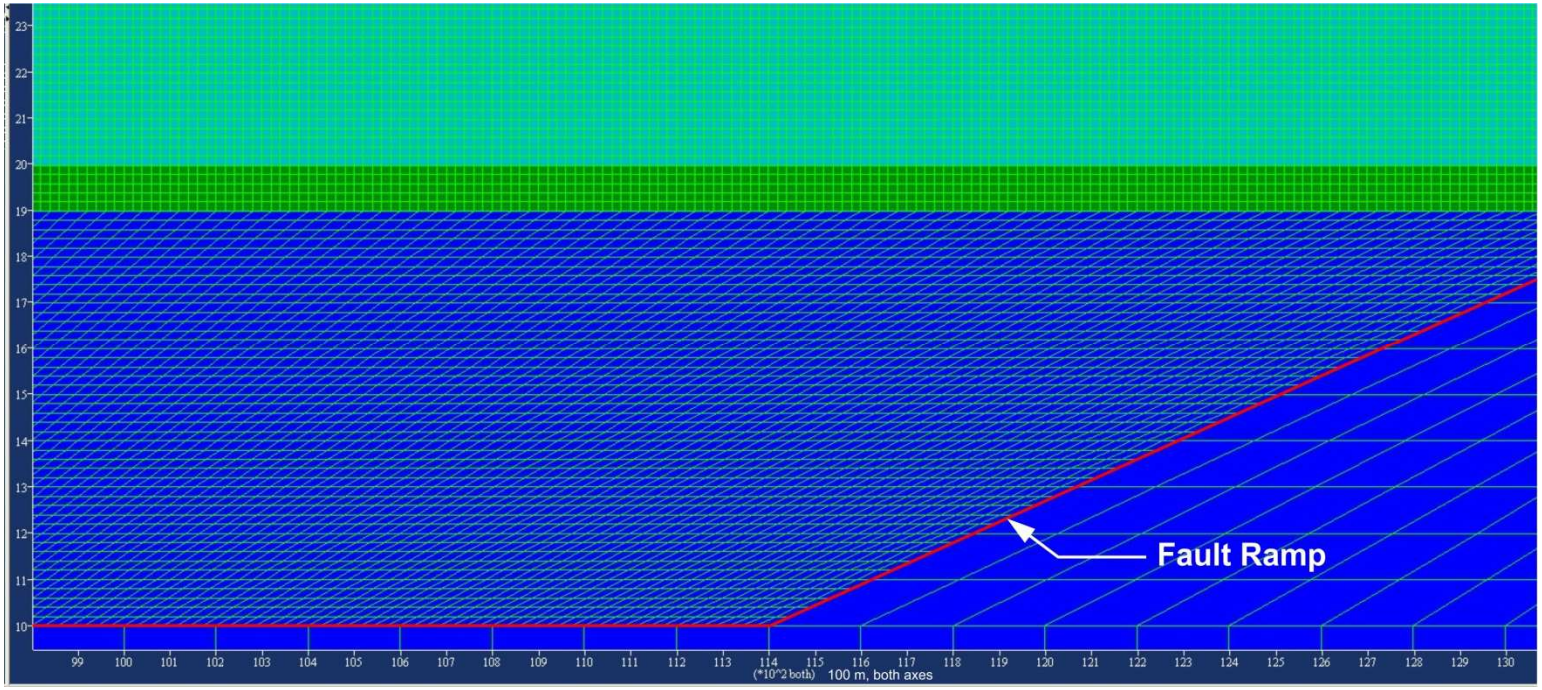

Figure 4.7: Element density differences between granite (blue) and overburden (green and above). Scale of axes – 100 m.

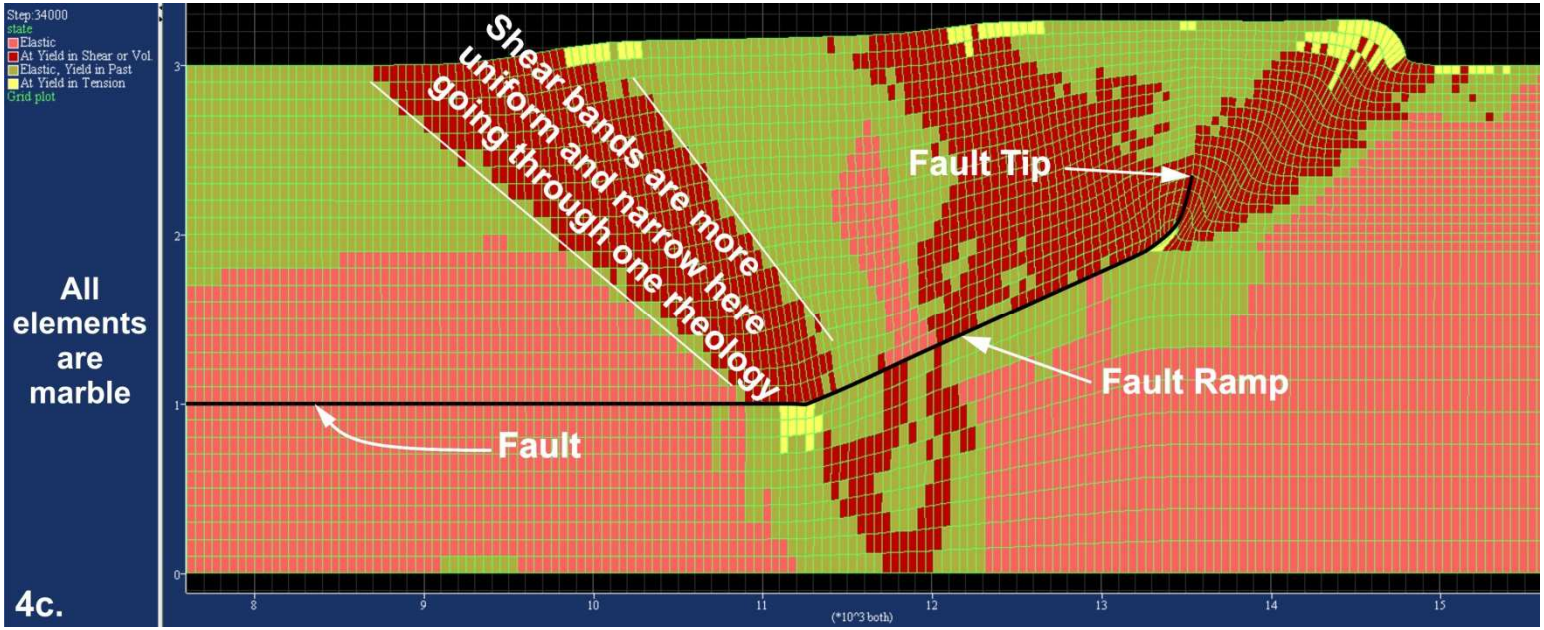

Figure 4.8: Model with marble rheology and equal mesh size above and below the fault. Scale of axes – 1 km.

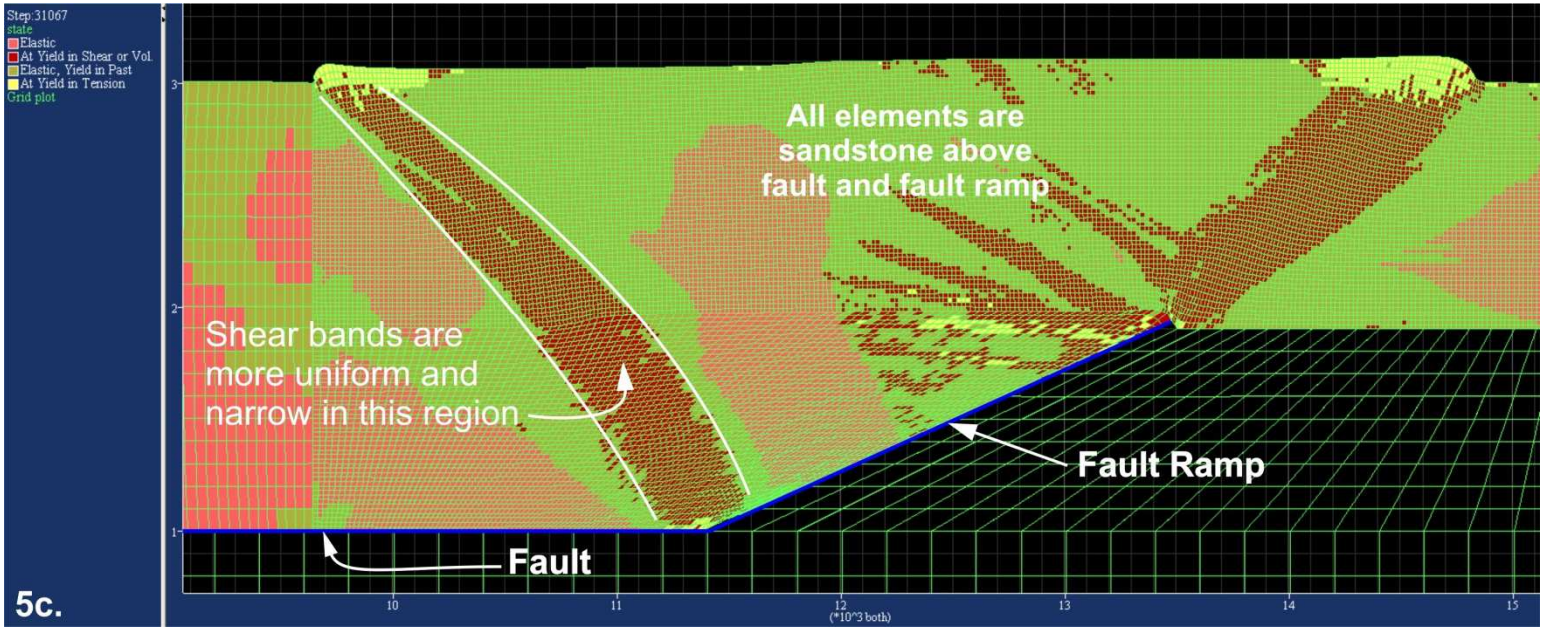

Figure 4.9: Model with sandstone rheology and larger mesh sizes below the fault. Scale of axes – 1 km.

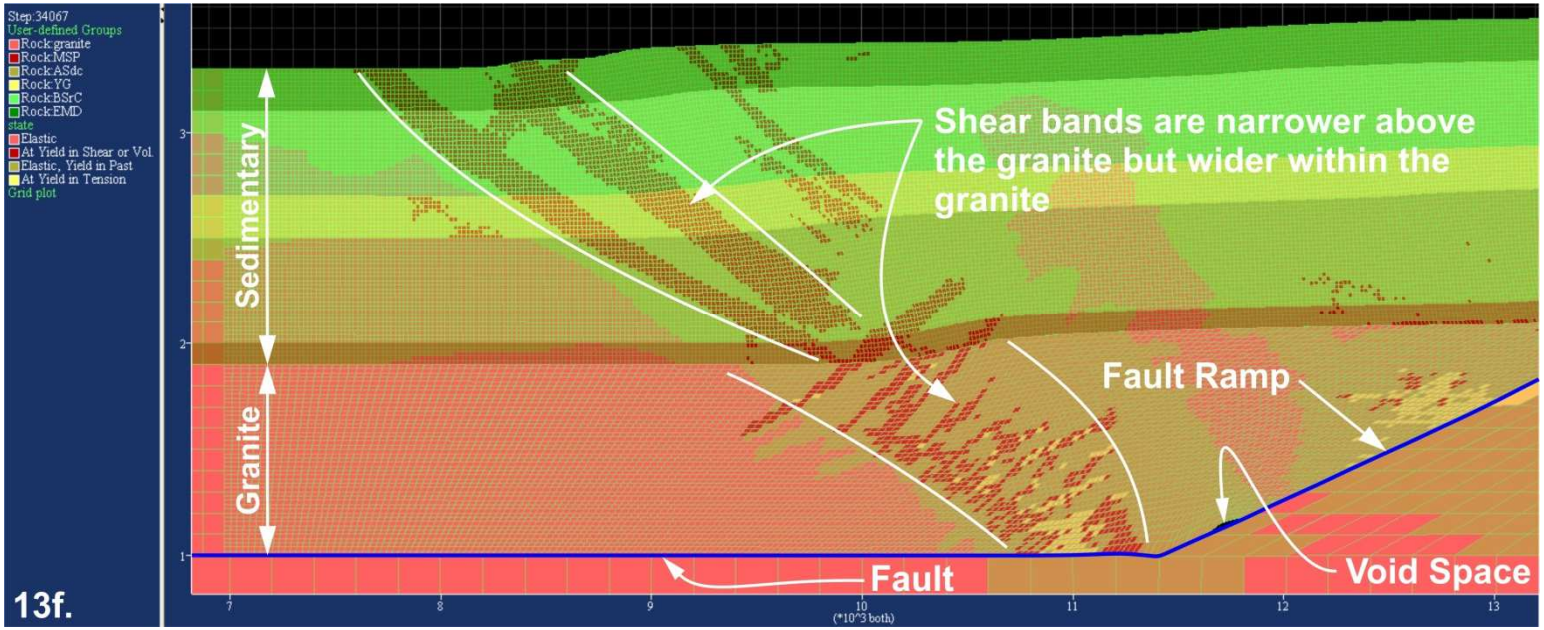

Figure 4.10: Model with study area stratigraphy; granite below and mixed beds above and larger mesh sizes below the fault.

Scale of axes – 1 km.

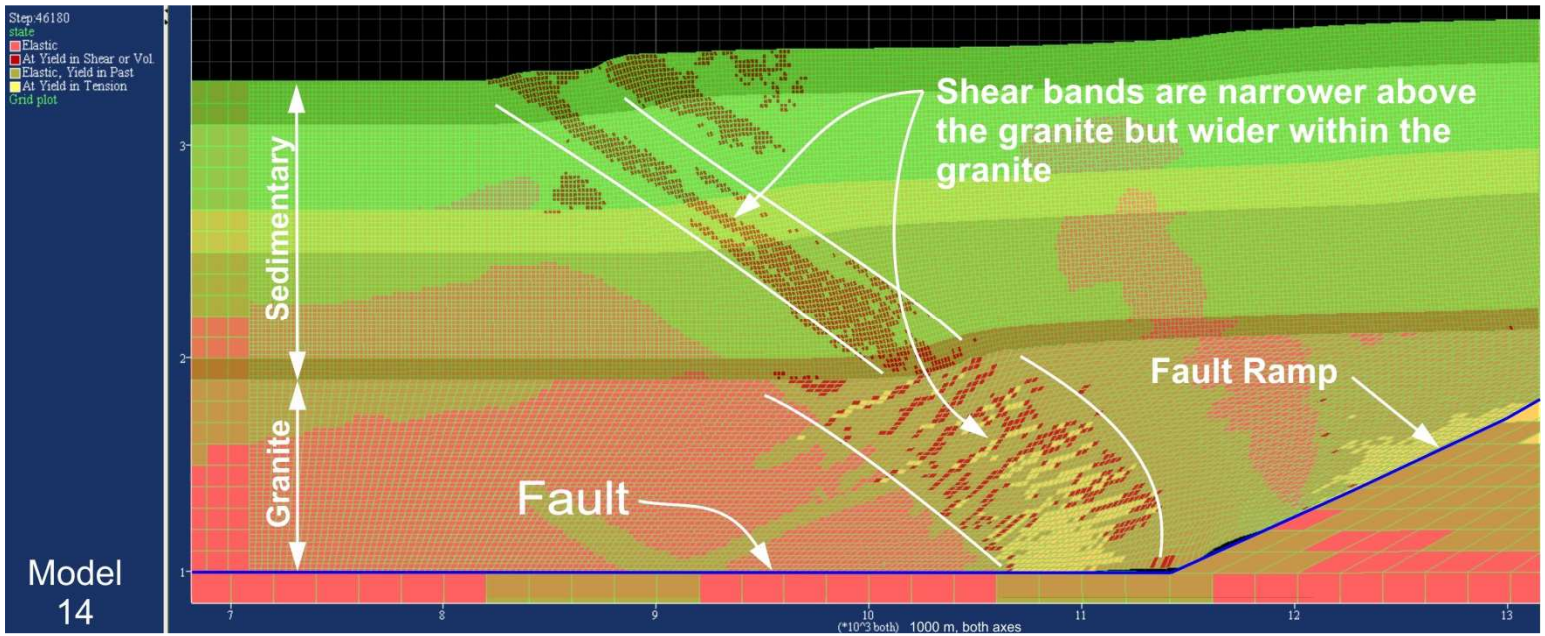

Figure 4.11: Model with study area stratigraphy; granite below and mixed beds above. Scale of axes – 1 km.

Chapter 5

Discussion

5.1 Strengths and Weaknesses of Model

Even though model simulation could not progress to a point where the fault propagates through the strata or develops a larger overturning, the models still produced uplift similar to the published cross section by Baltz (1972) (Figure 2.3). The shear band deformations originating at the fault bend and emerging at the surface near the location of the Medina Syncline is an expected similarity. The shear bands and the Medina Syncline are controlled by the position of the basement fault bend. If the bend was deeper or the ramp angle different, shear bands would generate the Medina Syncline somewhere else. The basement fault bends and flattens at whatever depth and ramp angle selected in this study. Future work could be performed to investigate model sensitivity of fault geometry and fault interface friction, as well as variation of the dilation angle and rock rheologies used.

5.2 Software Limitations

Large deformations are expected at the fault tip and each simulation reaches a point where the simulation will stop because an element is too distorted. FLAC will display an “invalid geometry” error code whenever this occurs. This can be overcome to some degree in the latest version of FLAC, version 7.0, which has recently been upgraded to handle problems similar to this, and is currently available for purchase. Since the version of FLAC used in this study cannot properly remesh to remove elements with invalid geometry, the model simulations are considered to be a rough approximation of the evolution of the faulting. With a remeshing algorithm, like the one included in FLAC version 7.0, this simulation could more closely model a fault propagation fold.

Appendix A

Table of Additional Models Run

Table A.1: Additional models run as shown in Appendix B

Additional Models Run			
Model Number	Number of Time-Steps Run	Number of Elements	Description
1	20,000	672	3 beds with interface between lower 2 beds & a fault going through top bed and middle bed.
1c	314,800	672	Same geometry but interface cuts through all beds from bottom to top; applied velocity all along left side of model; 314,800 steps.
1d	40	672	Same geometry but interface cuts through all beds from bottom to top; applied velocity all along left side of model; 40 steps; fault friction angle = 15°.
1e	31,220	672	Same geometry but interface cuts through all beds from bottom to top; applied velocity all along left side of model; 31,220 steps.
2	35,160	4874	Similar geometry but with a listric fault erupting at surface.
2d	0	4750	Initial position with 4 beds total, listric fault cutting thru 2 middle beds and ending at bottom of top bed, no applied velocity.
2e	30,101	4750	4 beds total, listric fault cutting thru 2 middle beds and ending at bottom of top bed, applied velocity across top three beds above fault flat.
2f	30,000	4750	4 beds total, listric fault cutting thru 2 middle beds and ending at bottom of top bed, applied velocity across two middle beds above fault flat.
2g	0	2,917	Initial position with 6 beds total, listric fault cutting thru 4 middle beds and ending at bottom of top bed, no applied velocity.
2h	59,748	2,917	6 beds total, listric fault cutting thru 4 middle beds and ending at bottom of top bed, applied velocity across top six beds above fault flat.
3	20,000	14,700	Fault propagation fold; equal number of elements split above and below fault; rock - marble w/ Mohr Coulomb plasticity; fault interface is applied vertically one element.
4	34,000	14,970	Fault propagation fold; equal number split above and below fault; rock - marble w/ Mohr Coulomb plasticity; fault interface is applied vertically five elements.
5	31,000	25,605	Fault propagation fold equal number split above and below fault; rock - sandstone w/ Mohr Coulomb plasticity; fault interface ends at top of ramp.

Table A.1 - Continued

6	29,217	25,605	Fault propagation fold; rock - granite & sandstone w/ Mohr Coulomb plasticity; fault interface ends at top of ramp. Mesh density above fault increases 9.4 km right of model left edge, low density below fault.
7	35,269	25,605	Fault propagation fold; rock - granite & sandstone w/ Mohr Coulomb plasticity; fault interface ends at top of ramp. Mesh density above fault increases 9.4 km right of model left edge, low density below fault.
8	31,726	25,605	Fault propagation fold; rock - granite & sandstone w/ Mohr Coulomb plasticity; fault interface ends at top of ramp. Mesh density above fault increases 9.4 km right of model left edge, low density below fault.
9	30,376	25,605	Fault propagation fold; 20 km long; rock - granite & sandstone w/ Mohr Coulomb plasticity; fault interface ends at top of ramp. Mesh density above fault increases 6.4 km right of model left edge, low density below fault.
10	32,541	38,868	Fault propagation fold; 20 km long; rock - granite & sandstone w/ Mohr Coulomb plasticity; fault interface ends at top of ramp. Mesh density above fault increases 5 km right of model left edge to 8.4 km, low density below fault.
11	31,541	38,868	Fault propagation fold; 20 km long; rock - granite & sandstone w/ Mohr Coulomb plasticity; fault interface ends at top of ramp. Mesh density above fault increases 5 km right of model left edge to 8.4 km, low density below fault.
12	33,560	46,308	Fault propagation fold; 21.6 km long; geometry with stratigraphy of study area w/ Mohr Coulomb plasticity; fault interface ends at top of ramp. Mesh density above fault increases 6.4 km right of model left edge to 11.4 km, low density below fault.
13	34,067	46,308	Fault propagation fold; 21.6 km long; geometry with stratigraphy of study area w/ Mohr Coulomb plasticity; fault interface ends at top of ramp. Mesh density above fault increases 6.4 km right of model left edge to 11.4 km, low density below fault.

Appendix B

Figures of Additional Models Run

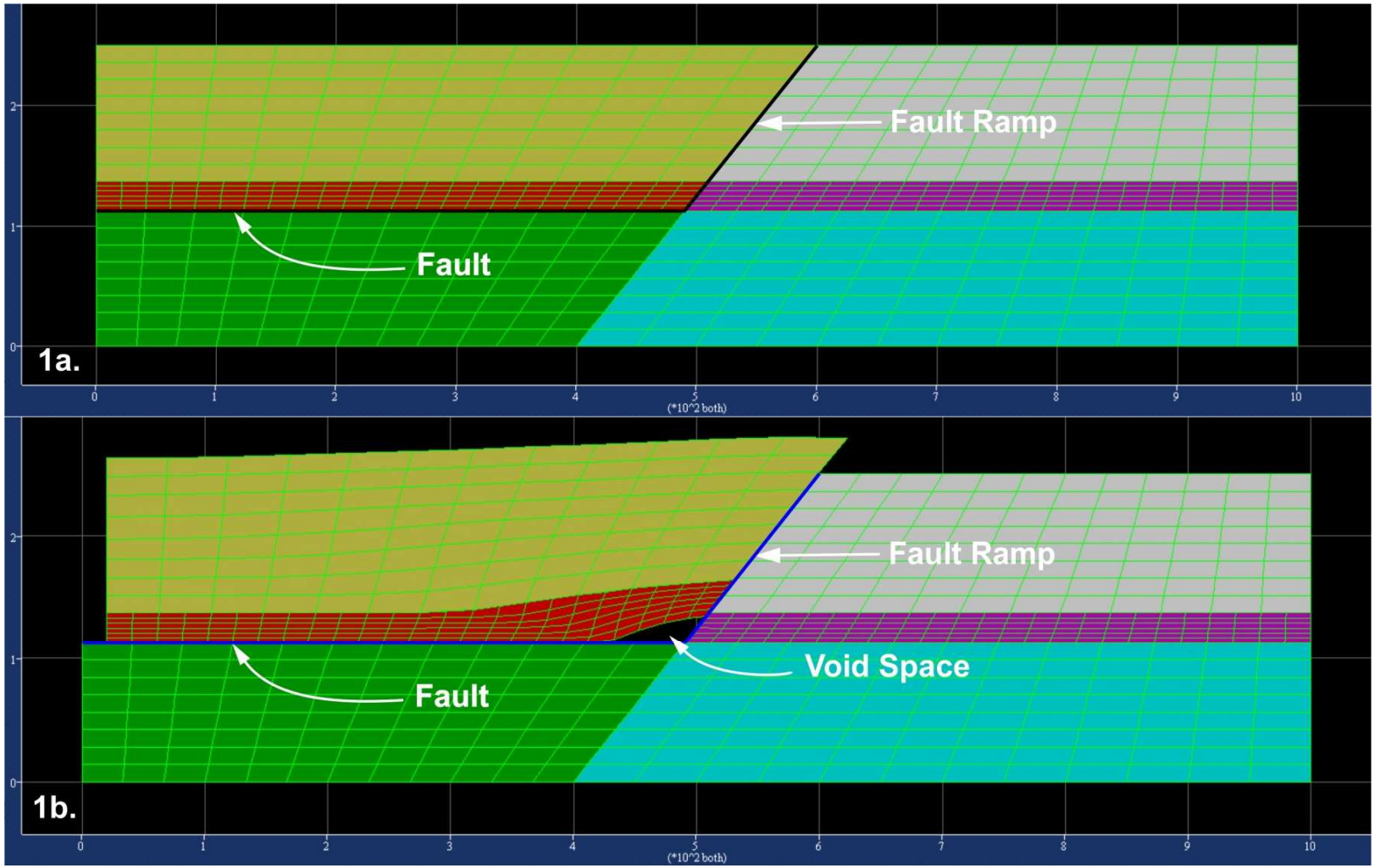

Figure B.1: Initial conditions - 1a and final – 1b; 0.02 m/s velocity applied only at top two beds. Scale of axes – 100 m.

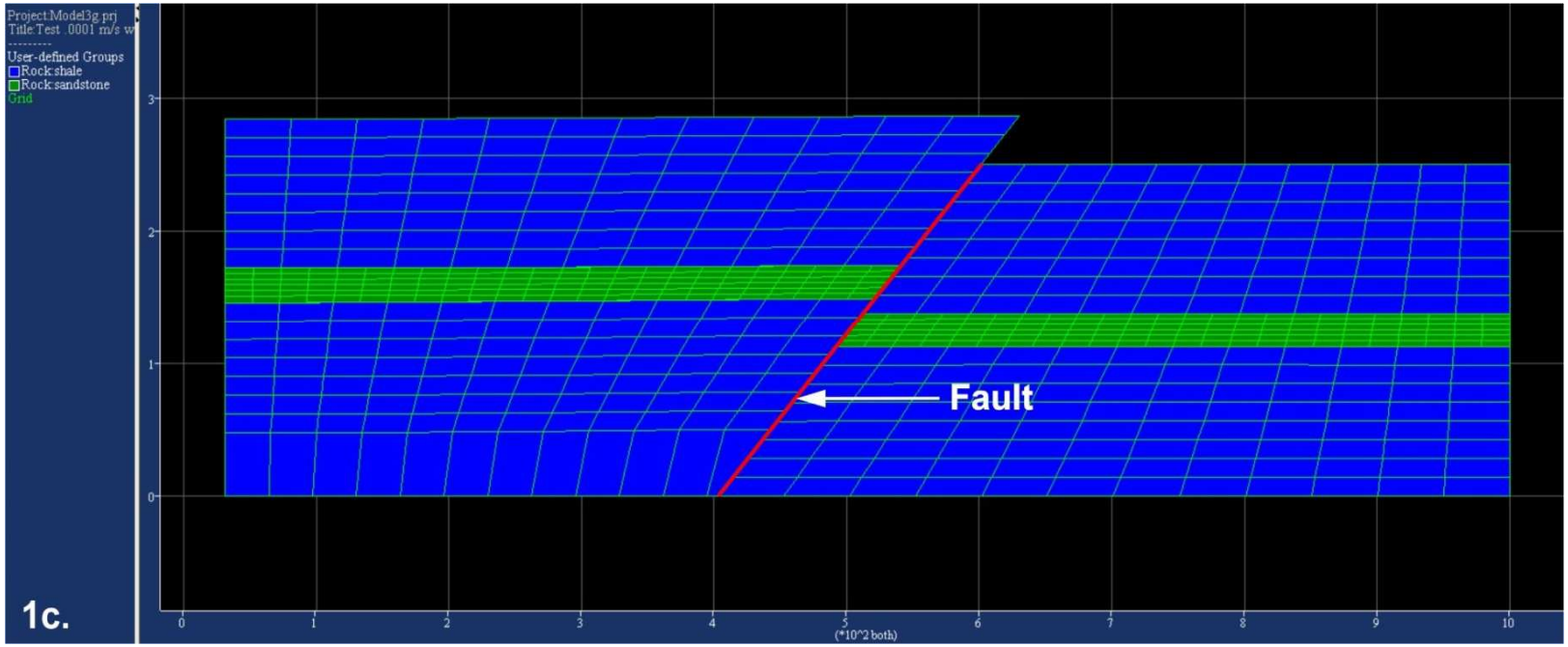

Figure B.2: Final model position; 0.02 m/s velocity applied to left hand end of model, top to bottom. Scale of axes – 100 m.

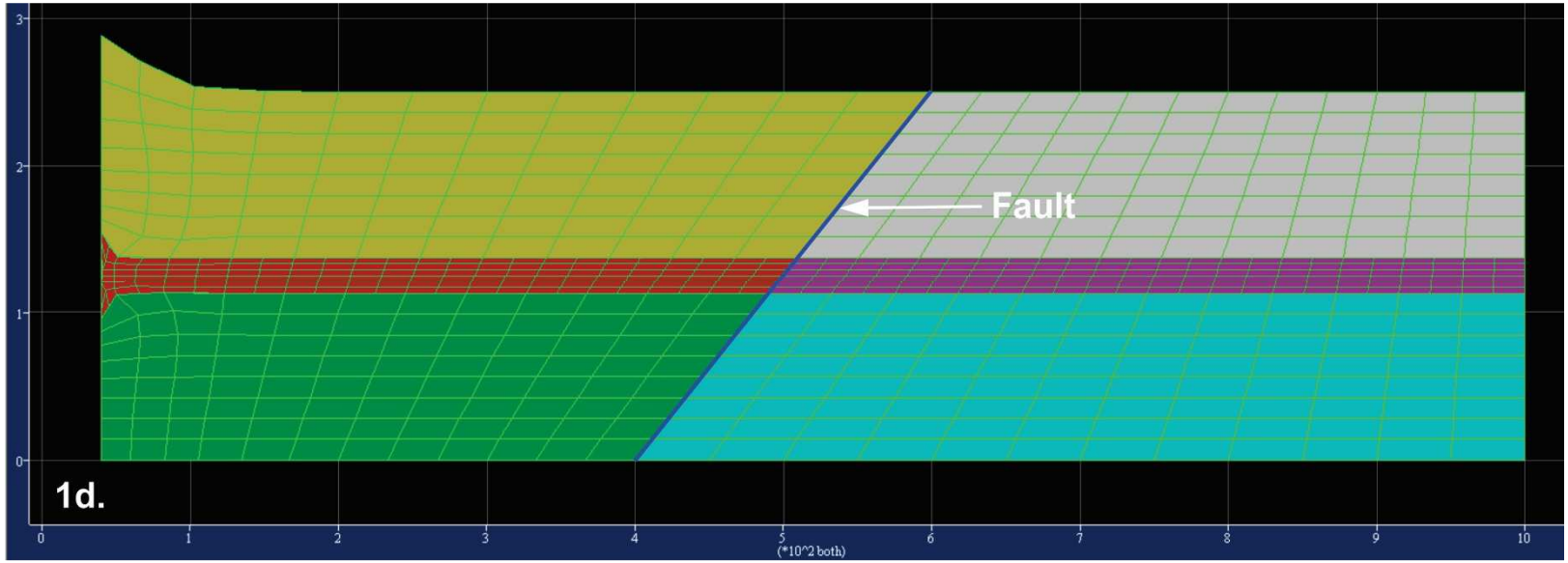

Figure B.3: Final model position; 0.02 m/s velocity applied to left hand end of model, top to bottom. Fault sliding not allowed. Scale of axes – 100 m.

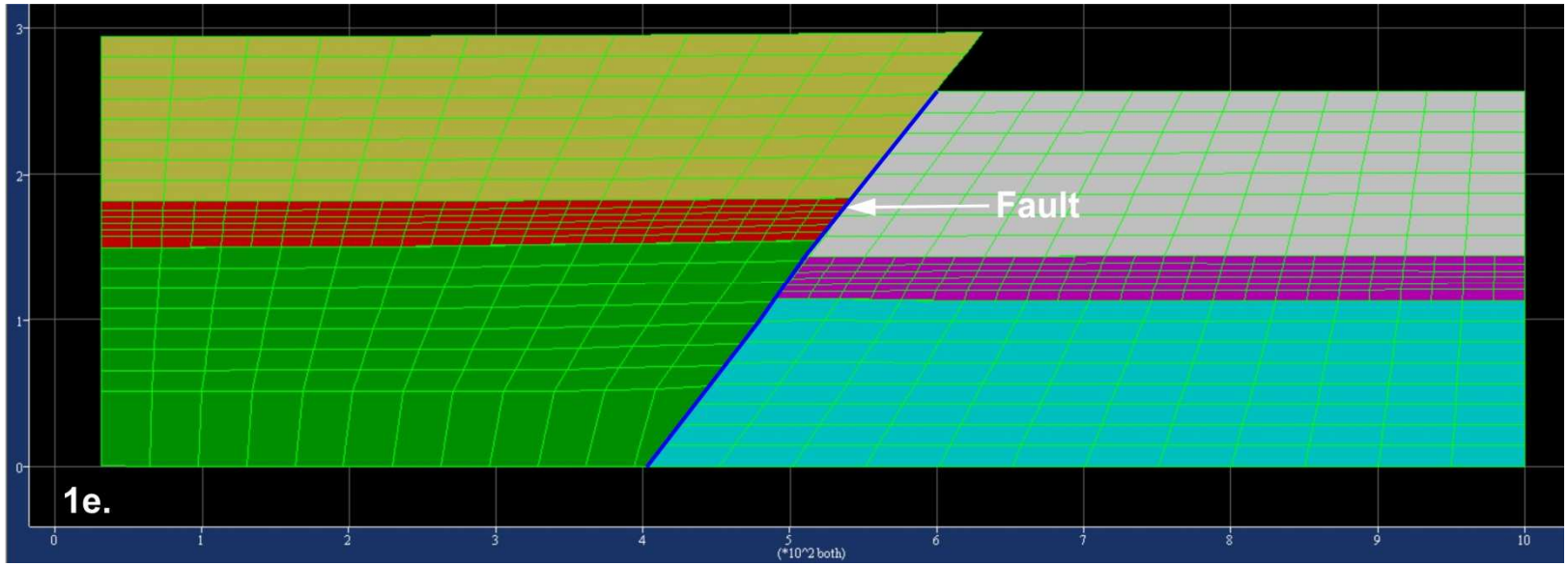

Figure B.4: Final model position; 0.02 m/s velocity applied to left hand end of model, top to bottom. Scale of axes – 100 m.

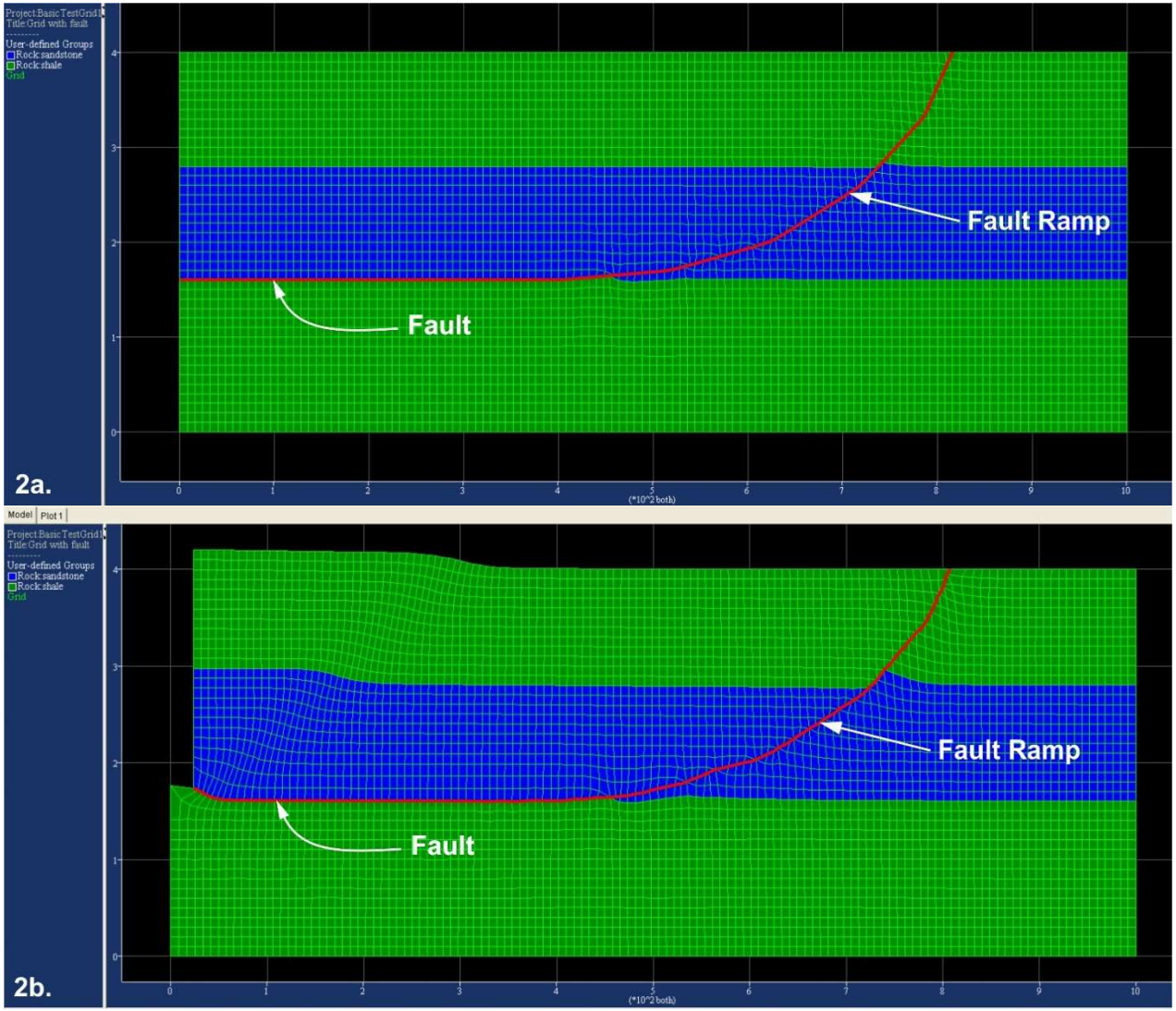

Figure B.5: Initial conditions - 2a and final - 2b. Sliding not allowed along fault surface. Scale of axes 100 m.

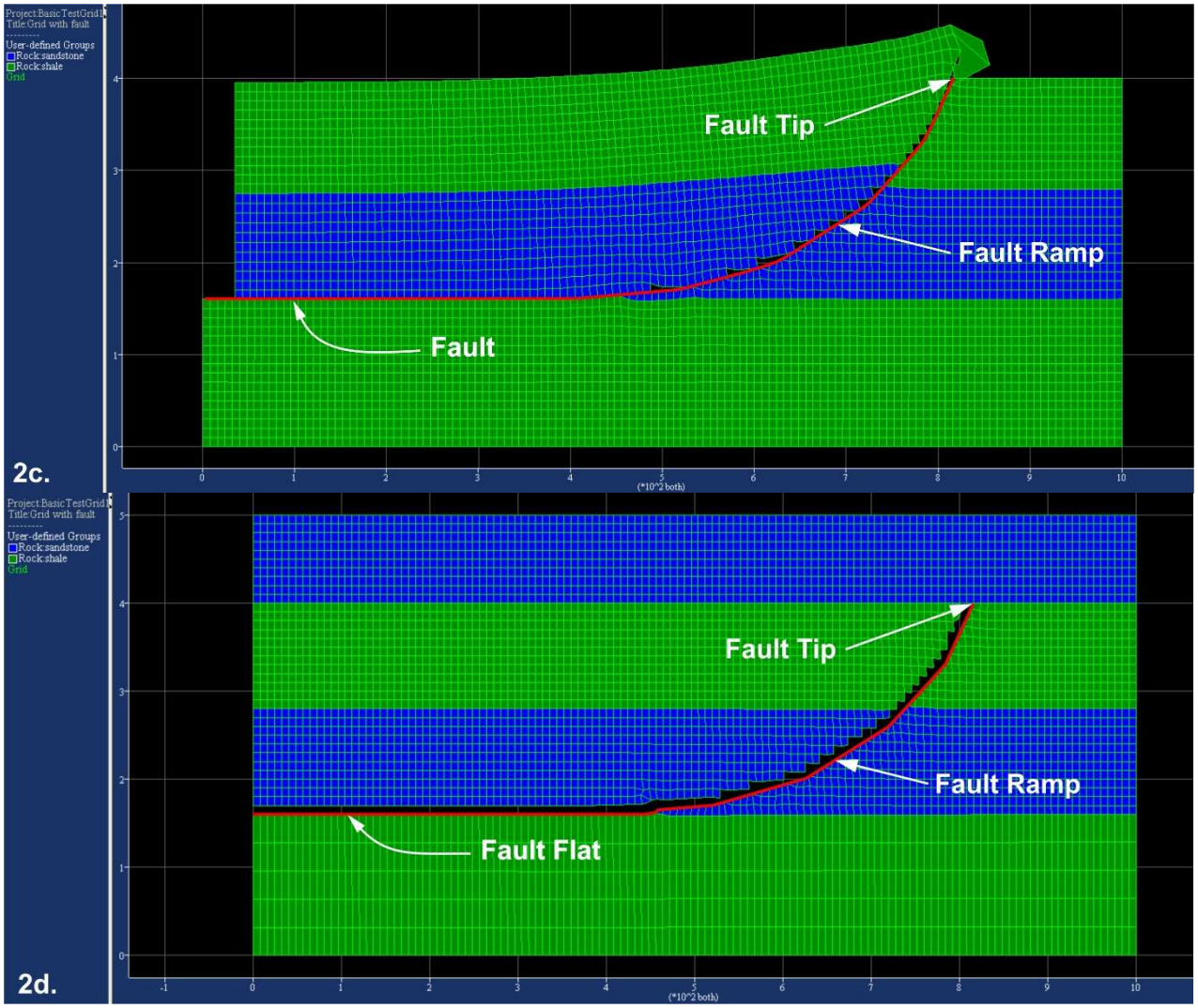

Figure B.6: Final positions; 2d has an extra bed of sandstone on top. Scale of axes – 100 m.

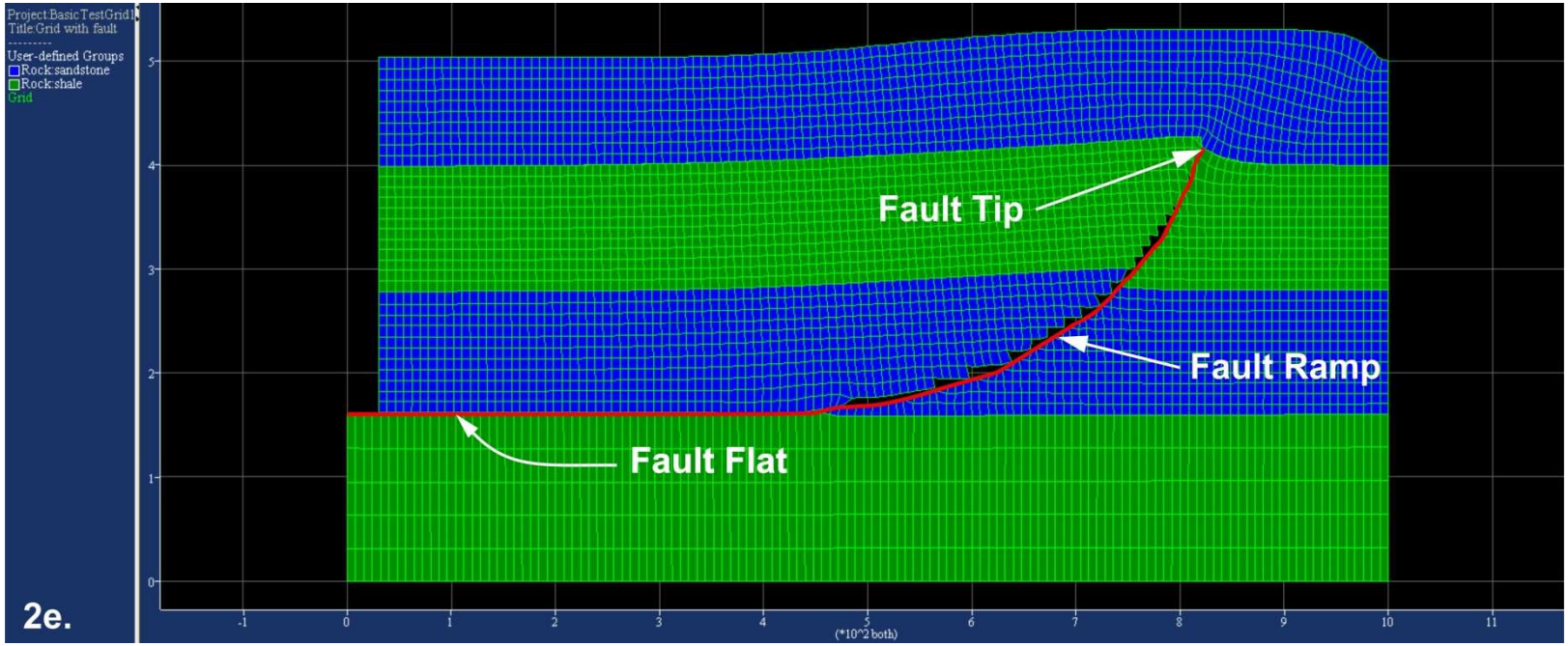

Figure B.7: Final model position; 0.02 m/s velocity applied only at top three beds. Scale of axes – 100 m.

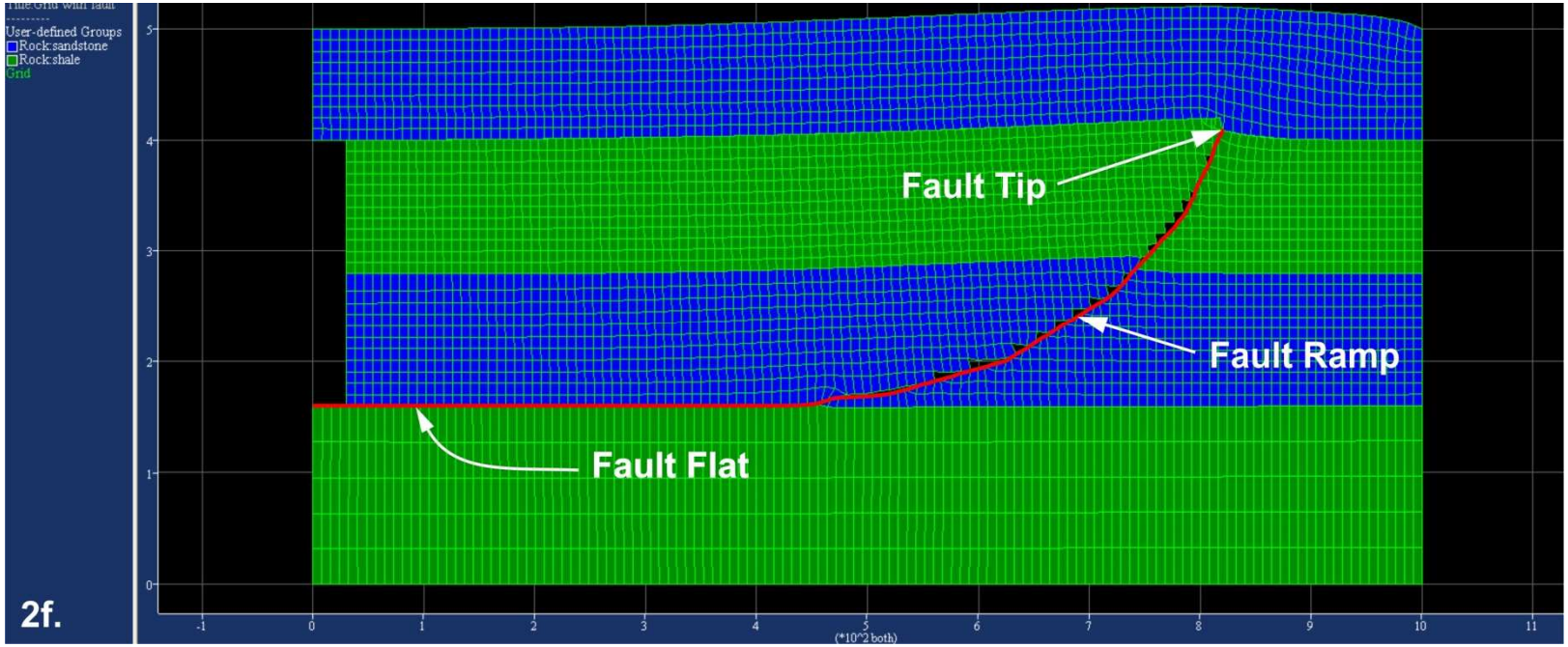

Figure B.8: Final position; extra bed of sandstone fixed stationary on top. Scale of axes – 100 m.

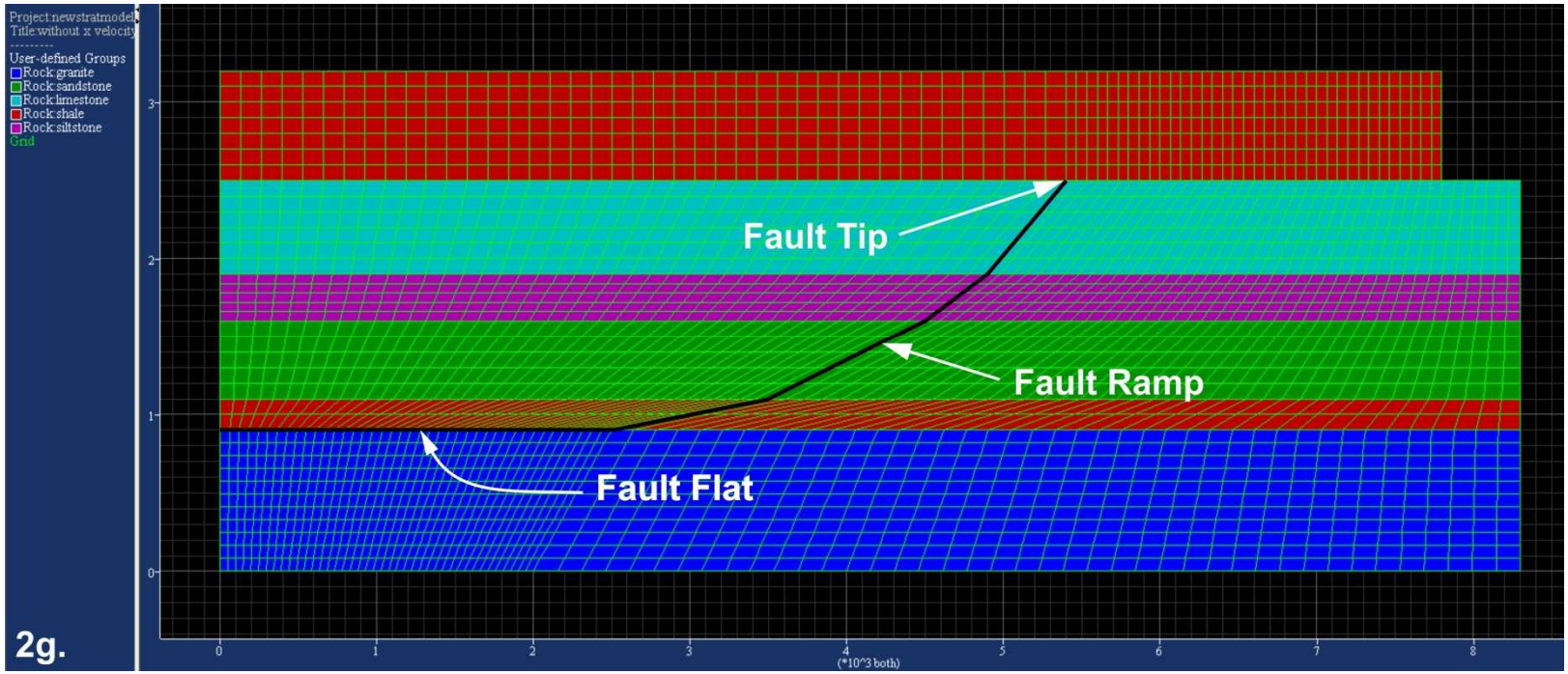

Figure B.9: Final position; mixed beds with shale fixed stationary on top. Scale of axes – 100 m.

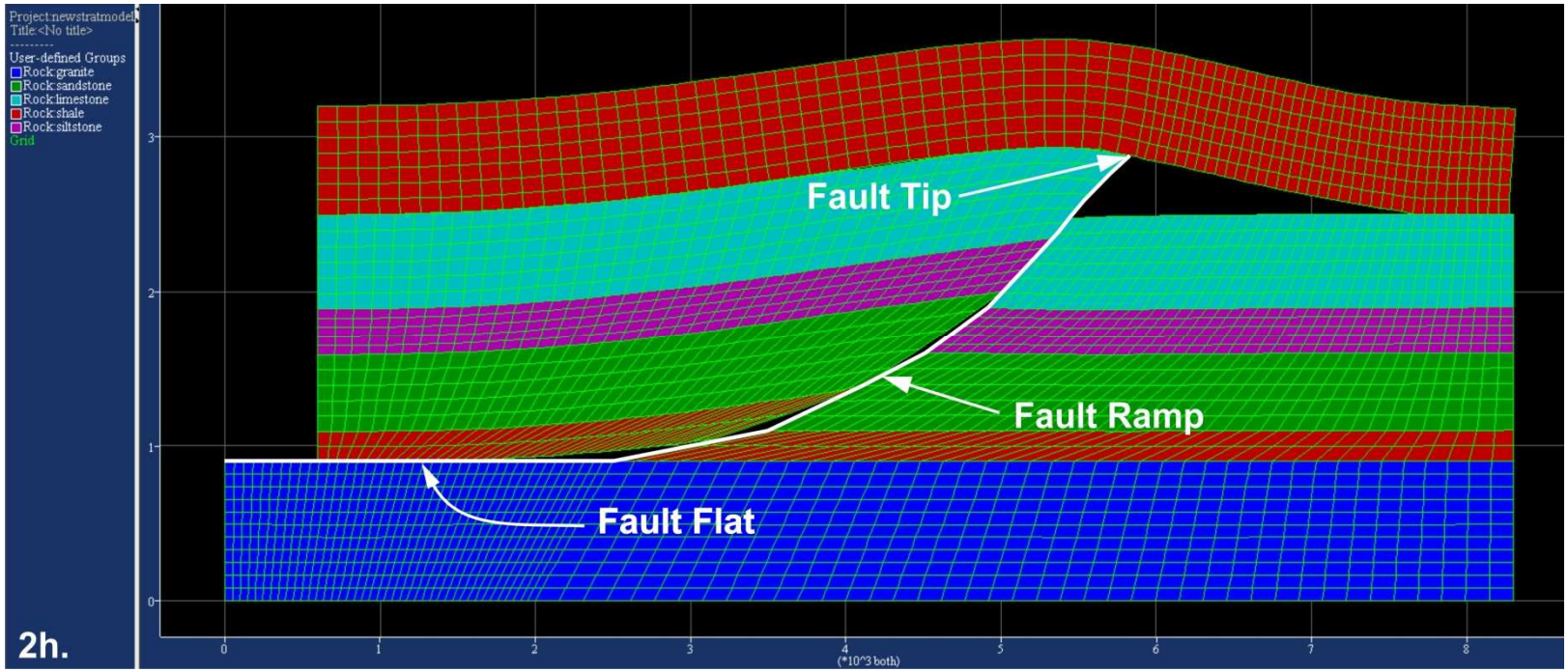

Figure B.10: Final position; mixed beds with shale fixed stationary top; 0.02 m/s velocity applied above fault flat. Scale of axes – 100 m.

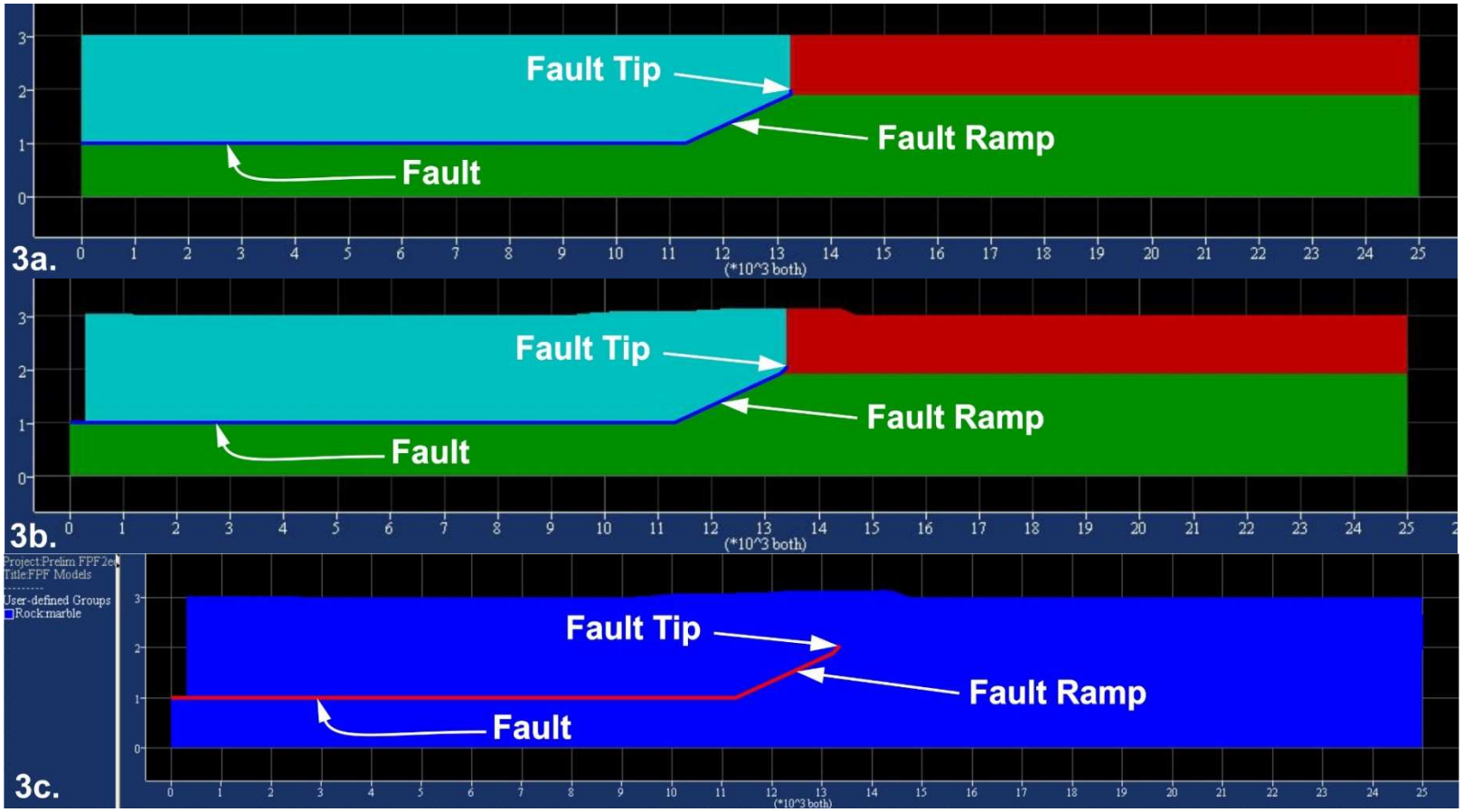

Figure B.11: Initial position - 3a and final - 3b and 3c; 3c shows model to be composed of all marble. Scale of axes 1 km.

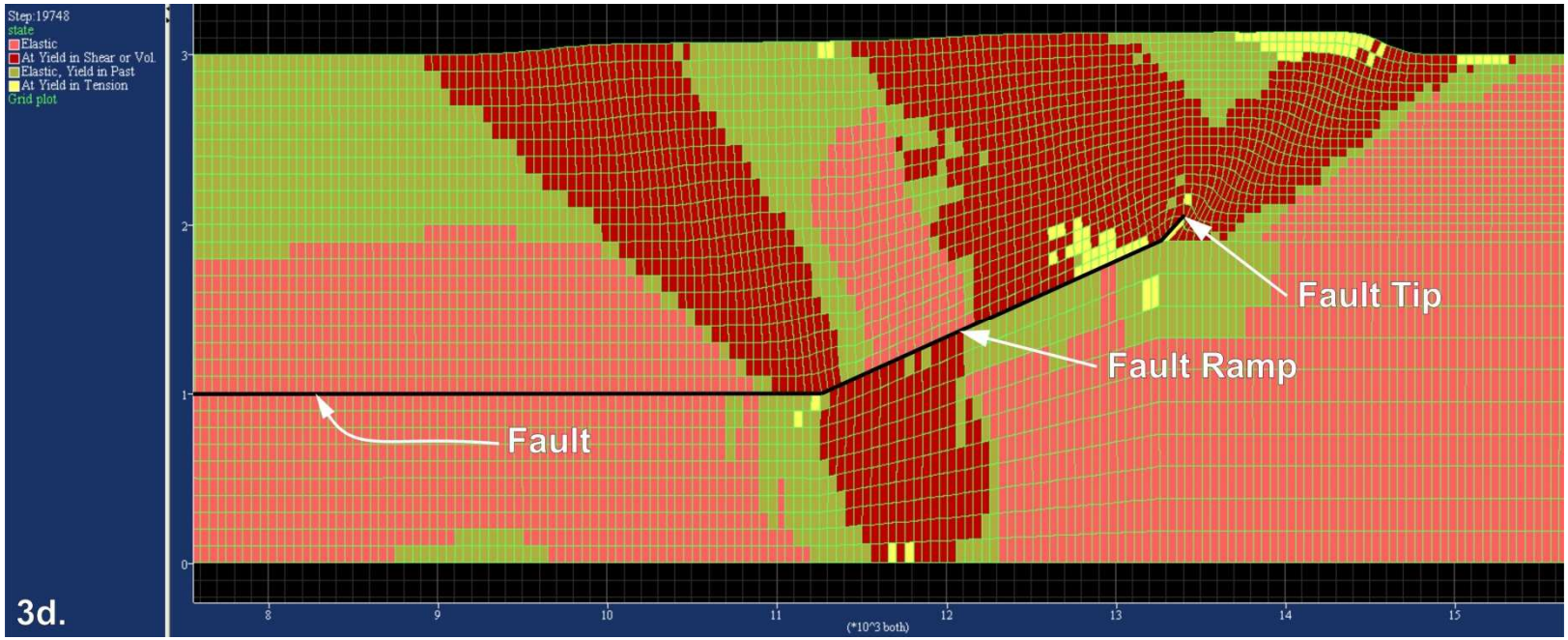

Figure B.12: Backthrust shear bands, model 3 (all marble). Shear bands are narrow and fault tip extends vertically. Scale of axes 1 km.

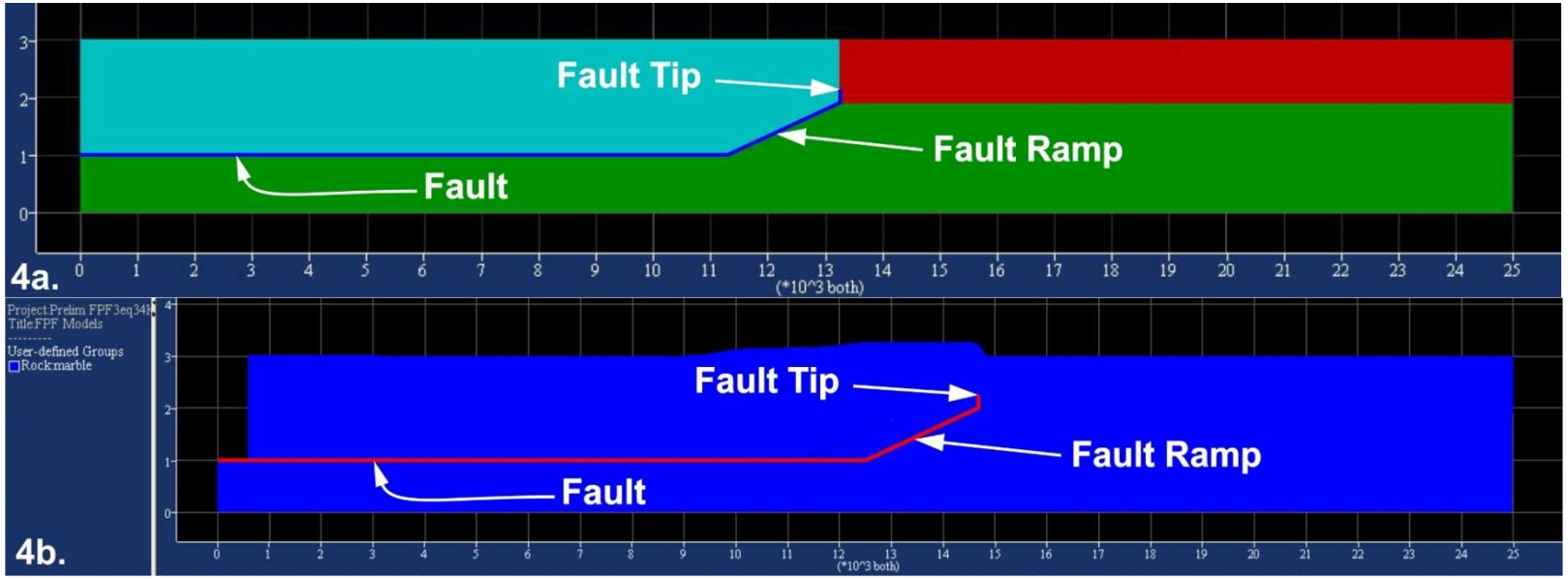

Figure B.13: Initial position - 4a and final - 4b, both models are all marble. Scale of axes 1 km.

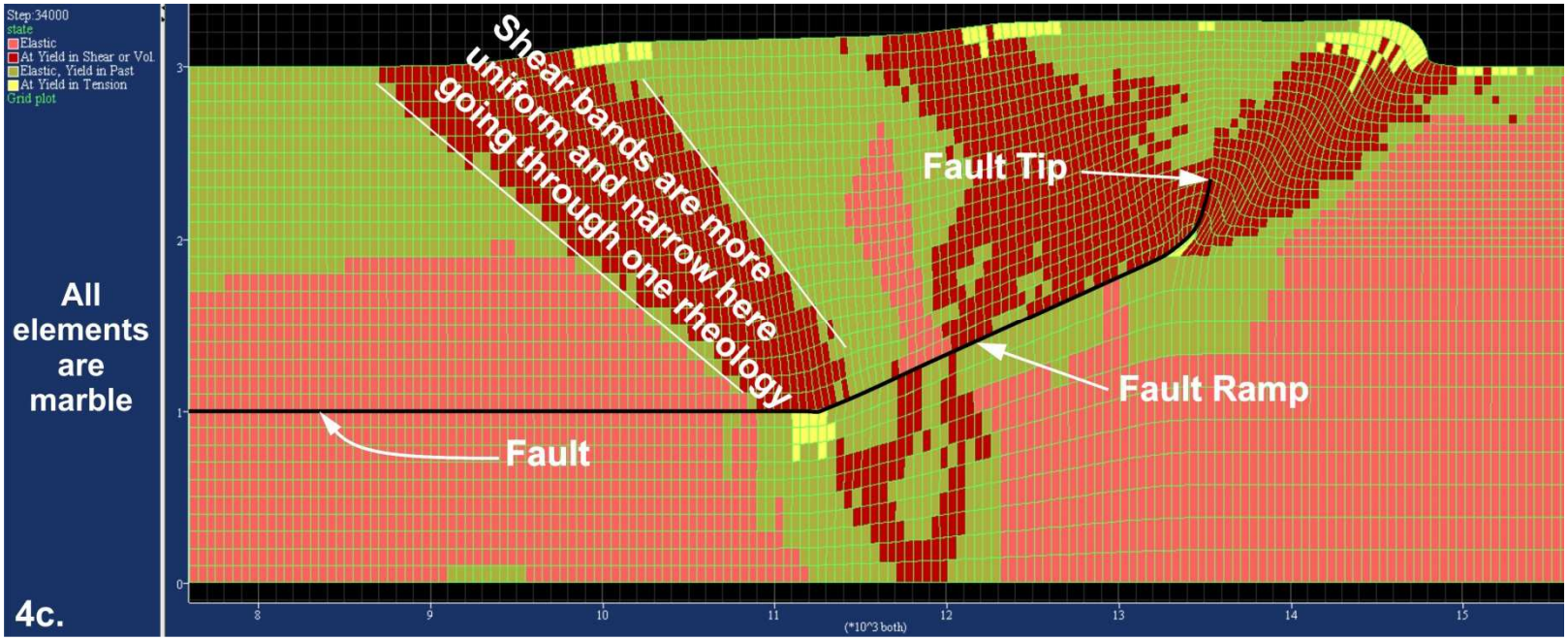

Figure B.14: Backthrust shear bands, model 4 (all marble). Shear bands are narrow and fault tip extends vertically. Scale of axes 1 km.

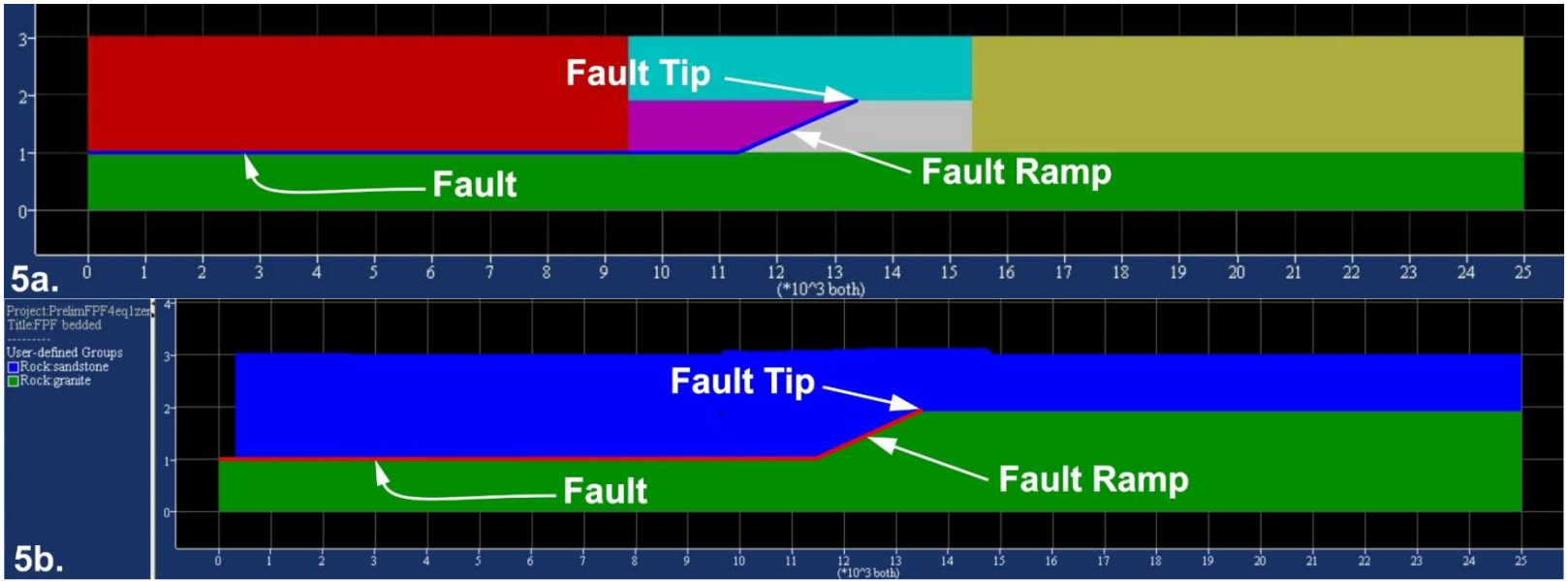

Figure B.15: Initial position - 5a and final - 5b; all sandstone above fault. Scale of axes 1 km.

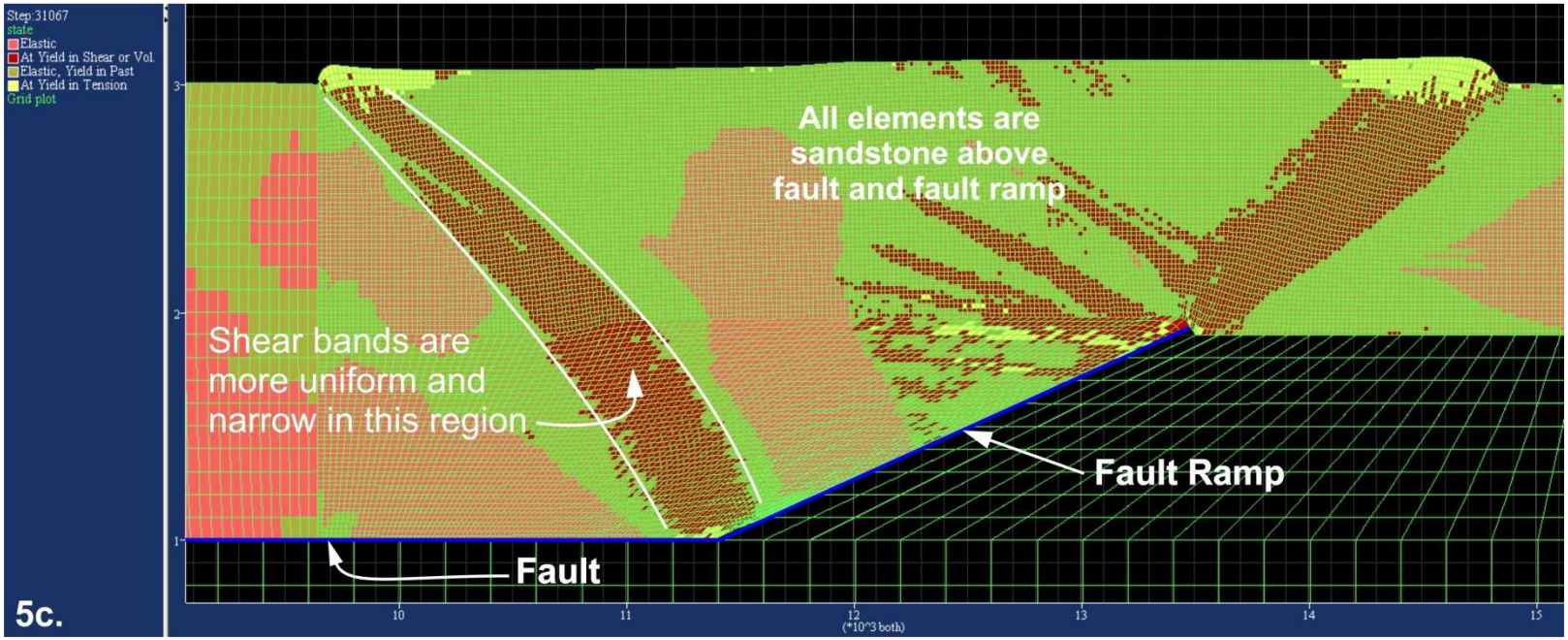

Figure B.16: Backthrust shear bands, model 5; all sandstone above fault. Shear bands are narrow. Scale of axes – 1 km.

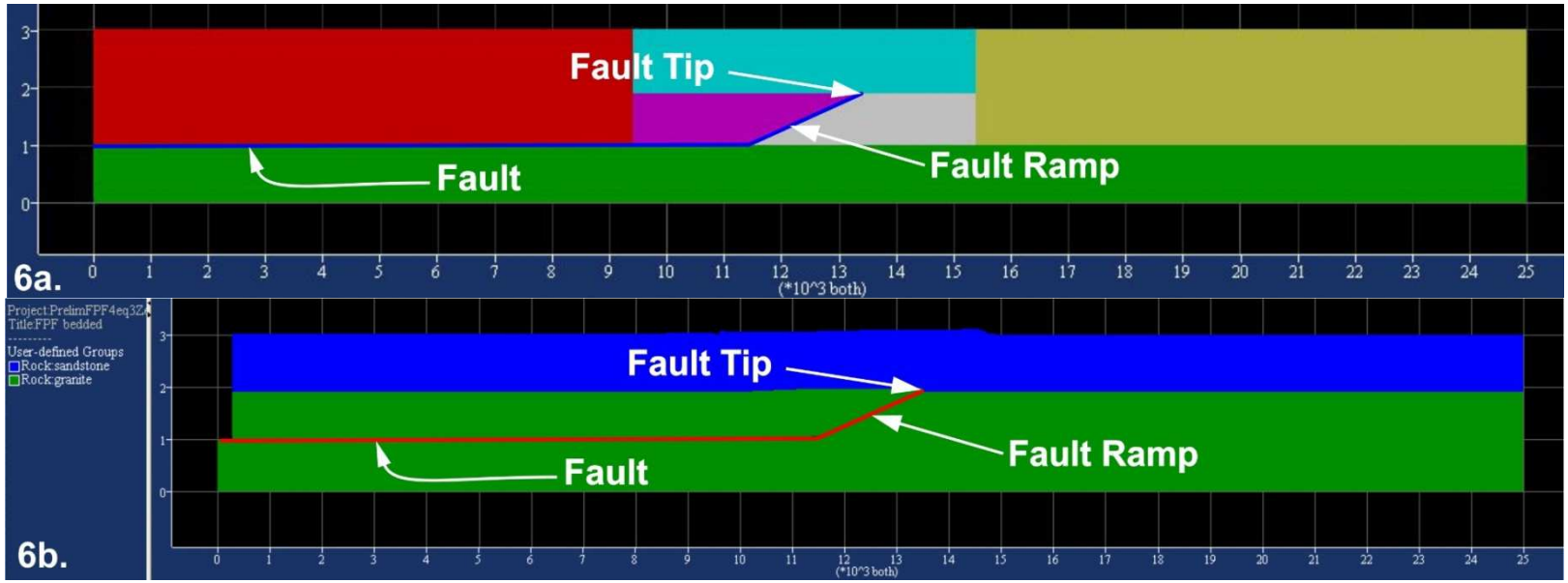

Figure B.17: Initial position - 6a and final - 6b; granite and sandstone above fault. Scale of axes 1 km.

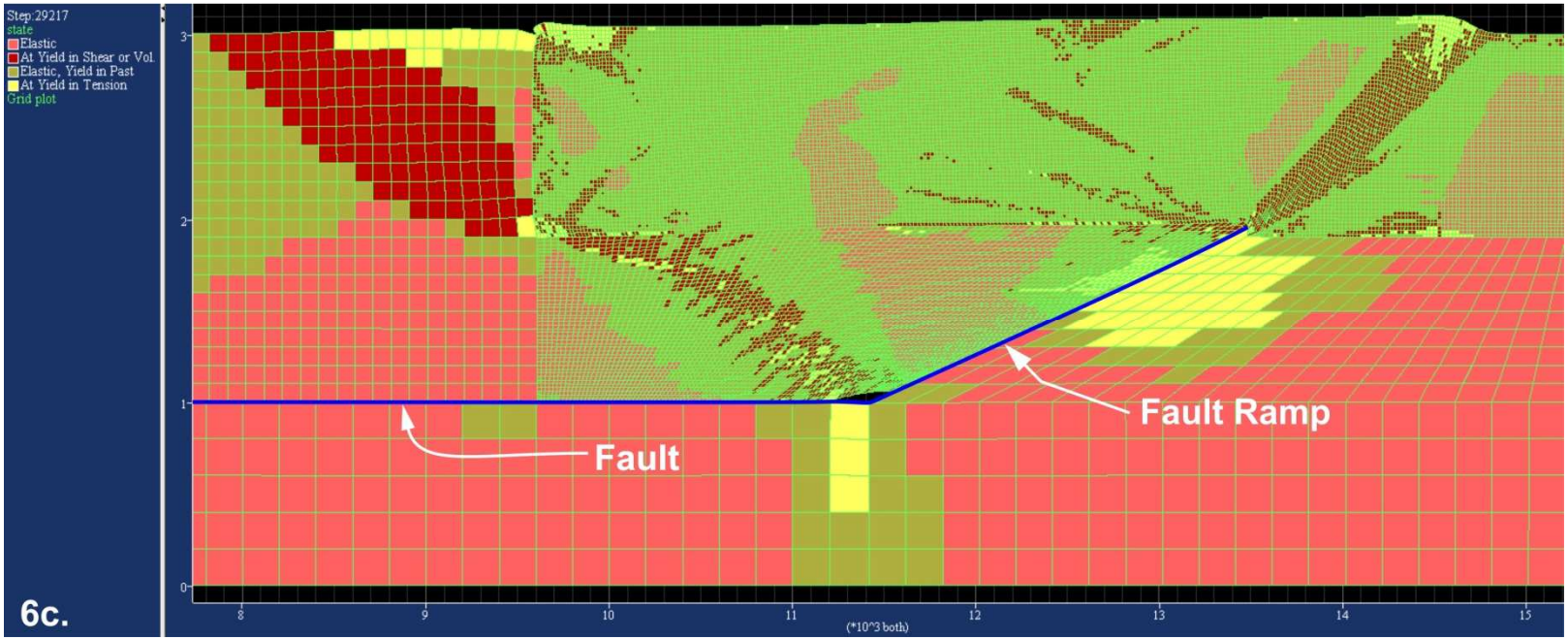

Figure B.18: Backthrust shear bands, model 6; granite and sandstone above fault. Shear bands; wider in granite. Scale of axes - 1 km.

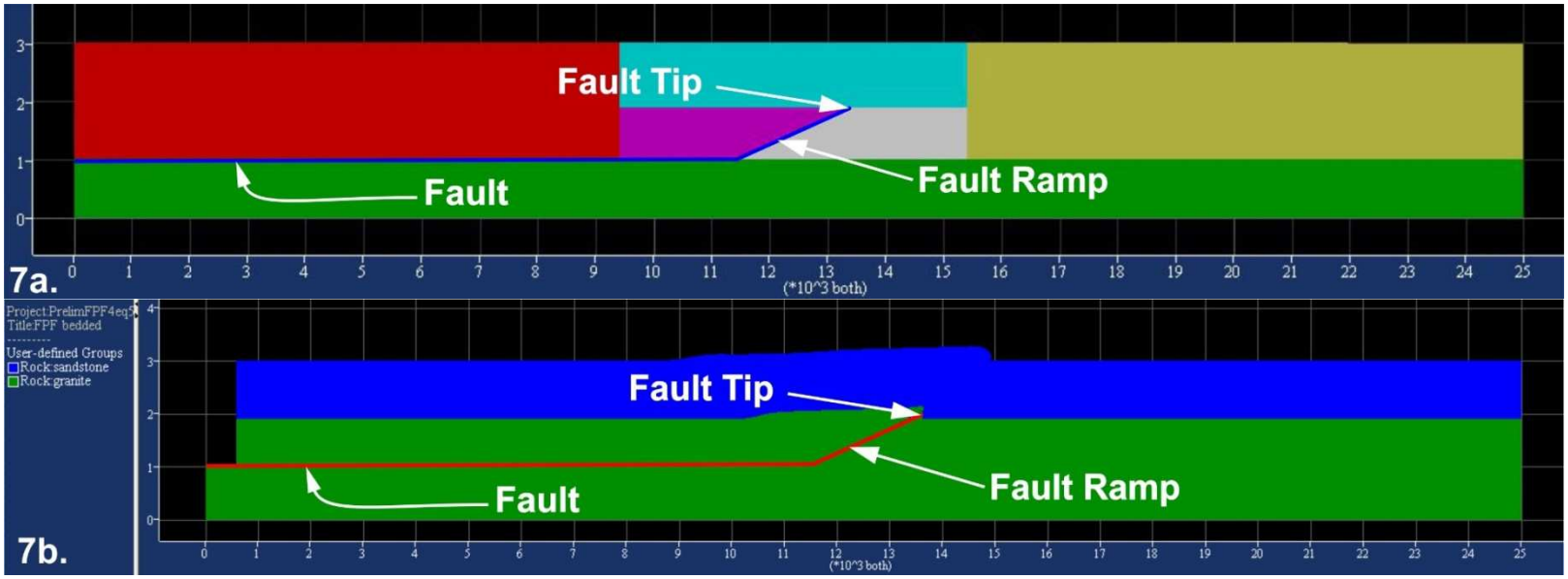

Figure B.19: Initial position - 7a and final - 7b; granite and sandstone above fault. Scale of axes – 1 km.

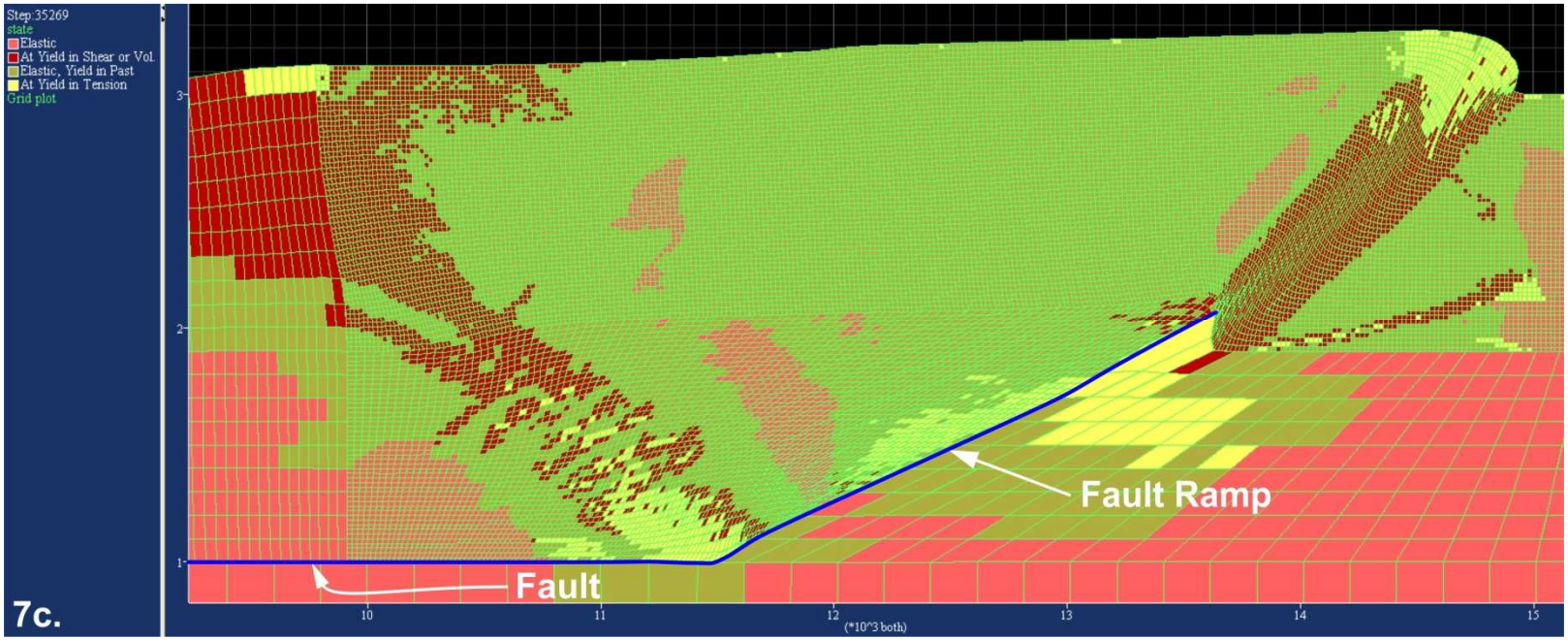

Figure B.20: Backthrust shear bands, model 7; granite and sandstone above fault. Shear bands are wider. Scale of axes – 1 km.

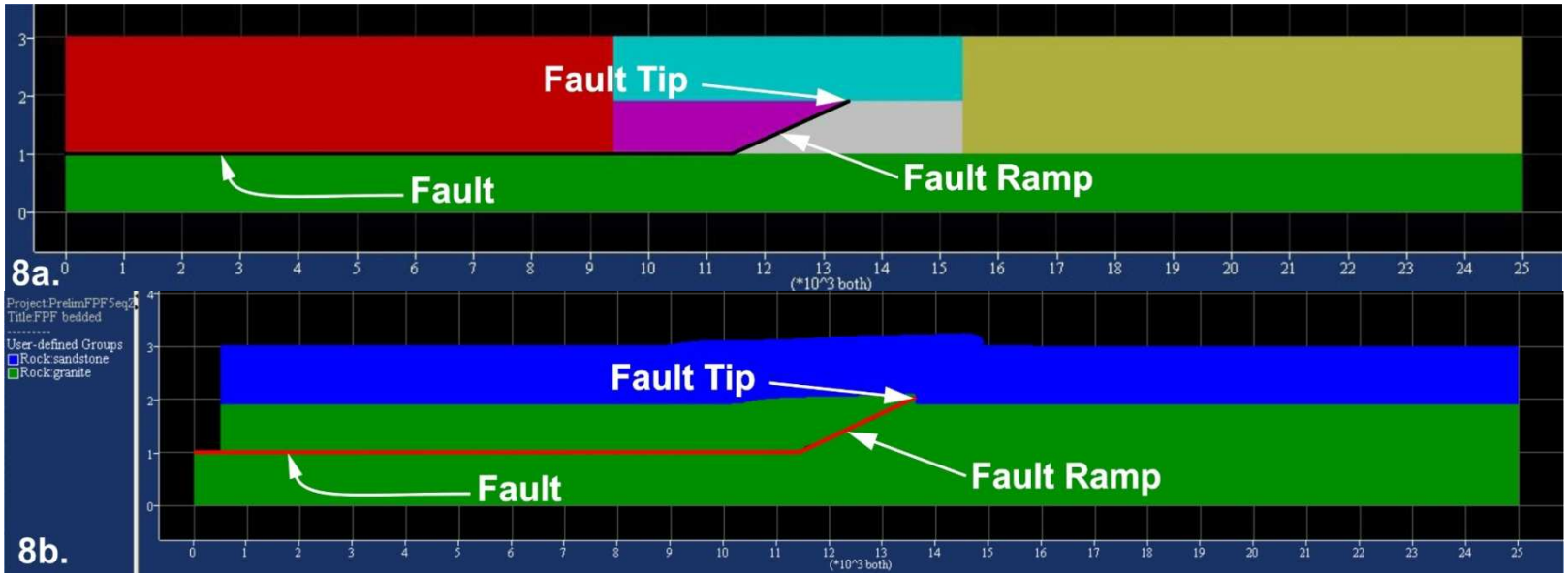

Figure B.21: Initial position - 8a and final - 8b; granite and sandstone above fault. Scale of axes – 1 km.

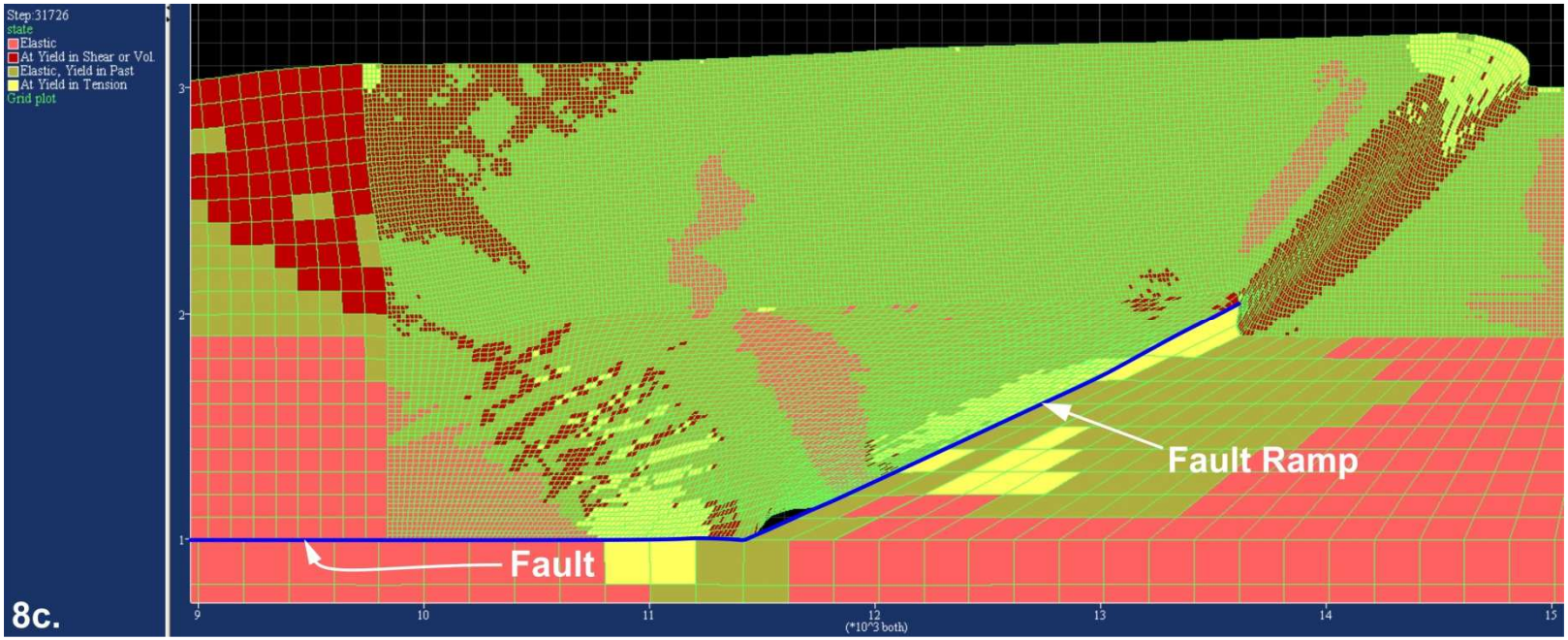

Figure B.22: Backthrust shear bands, model 8; granite and sandstone above fault. Shear bands are wider. Scale of axes – 1 km.

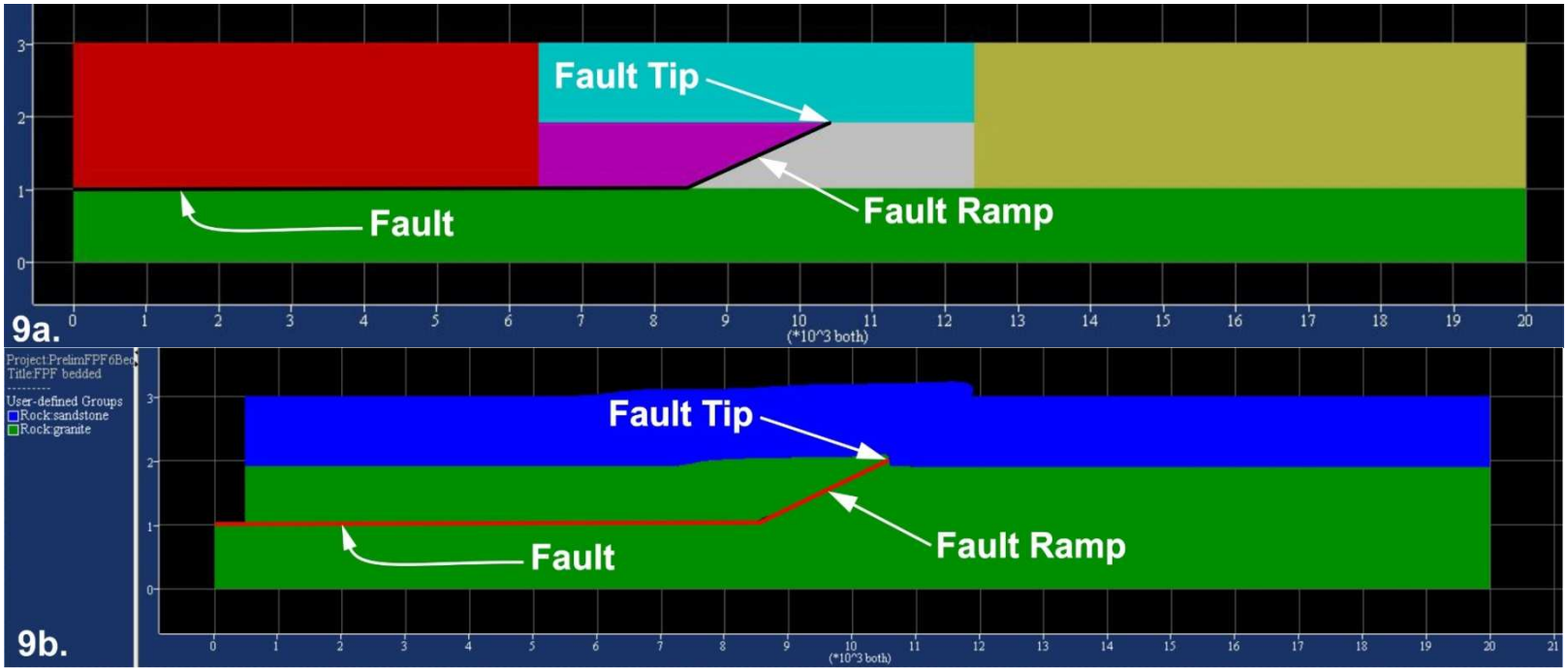

Figure B.23: Initial position - 9a and final - 9b; granite and sandstone above fault. Scale of axes 1 km.

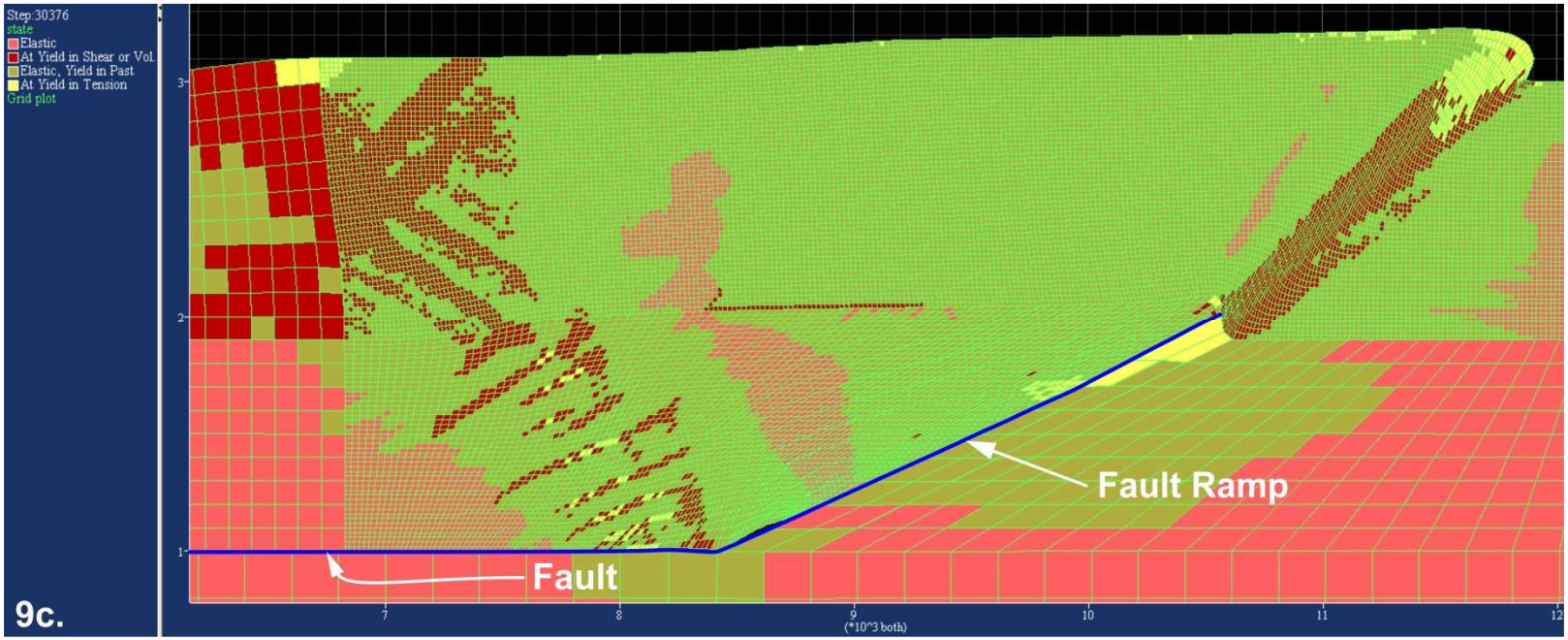

Figure B.24: Backthrust shear bands, model 9; granite and sandstone above fault. Shear bands are wider. Scale of axes – 1 km.

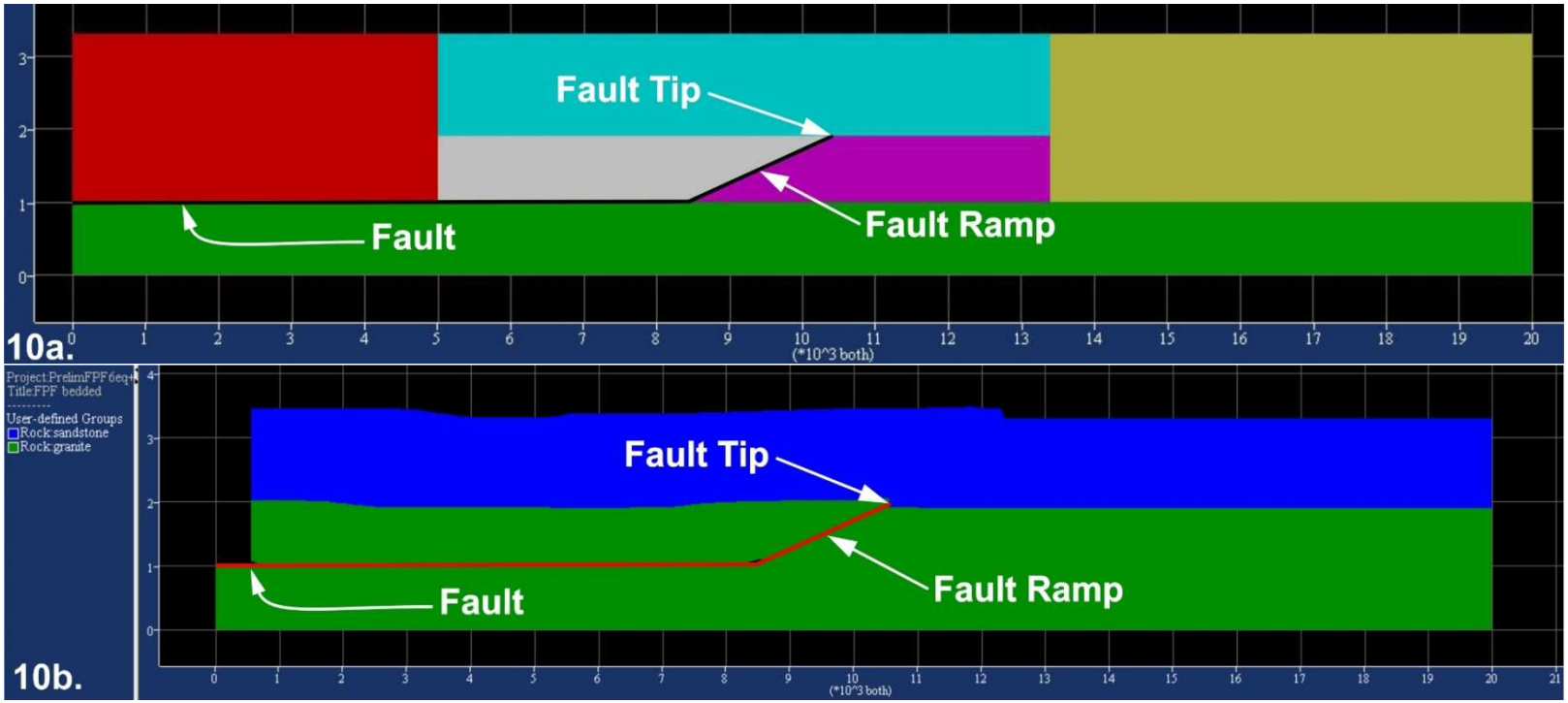

Figure B.25: Initial position - 10a and final - 10b; granite and sandstone above fault. Scale of axes – 1 km.

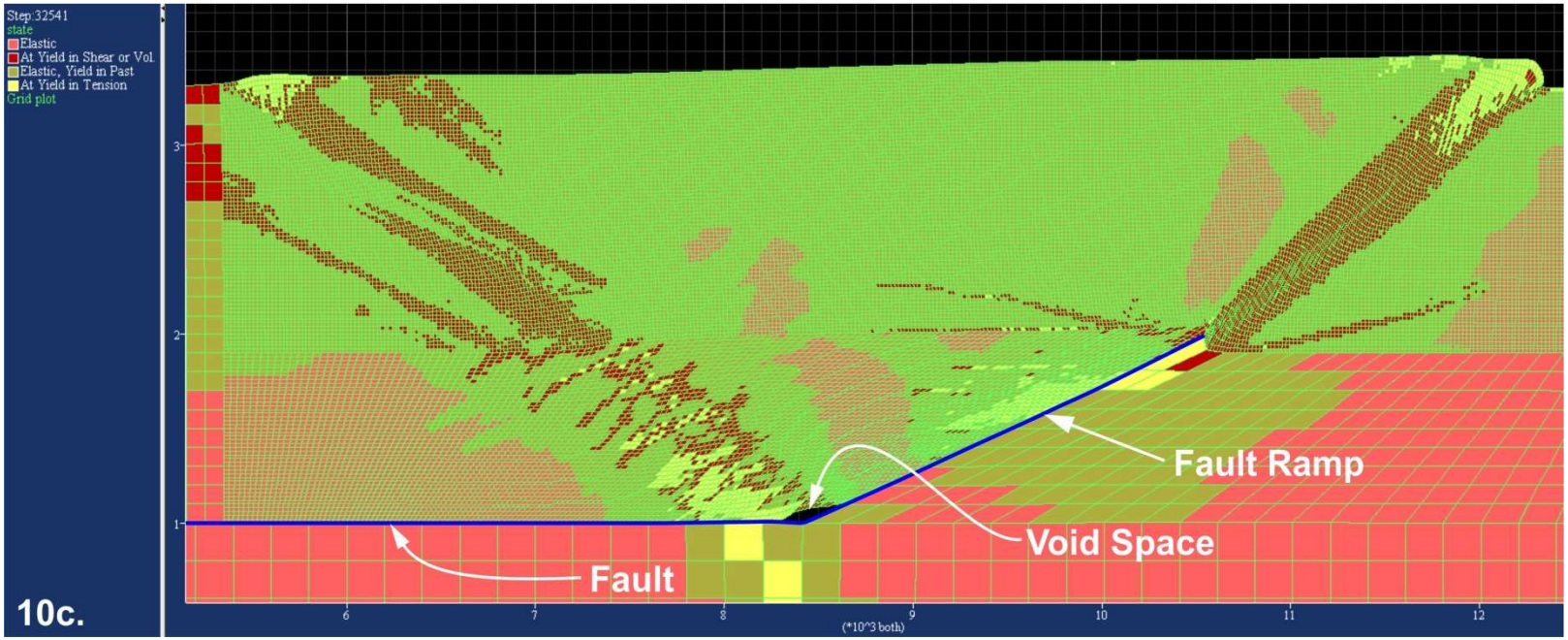

Figure B.26: Backthrust shear bands, model 10; granite and sandstone above fault. Shear bands are wider. Scale of axes – 1 km.

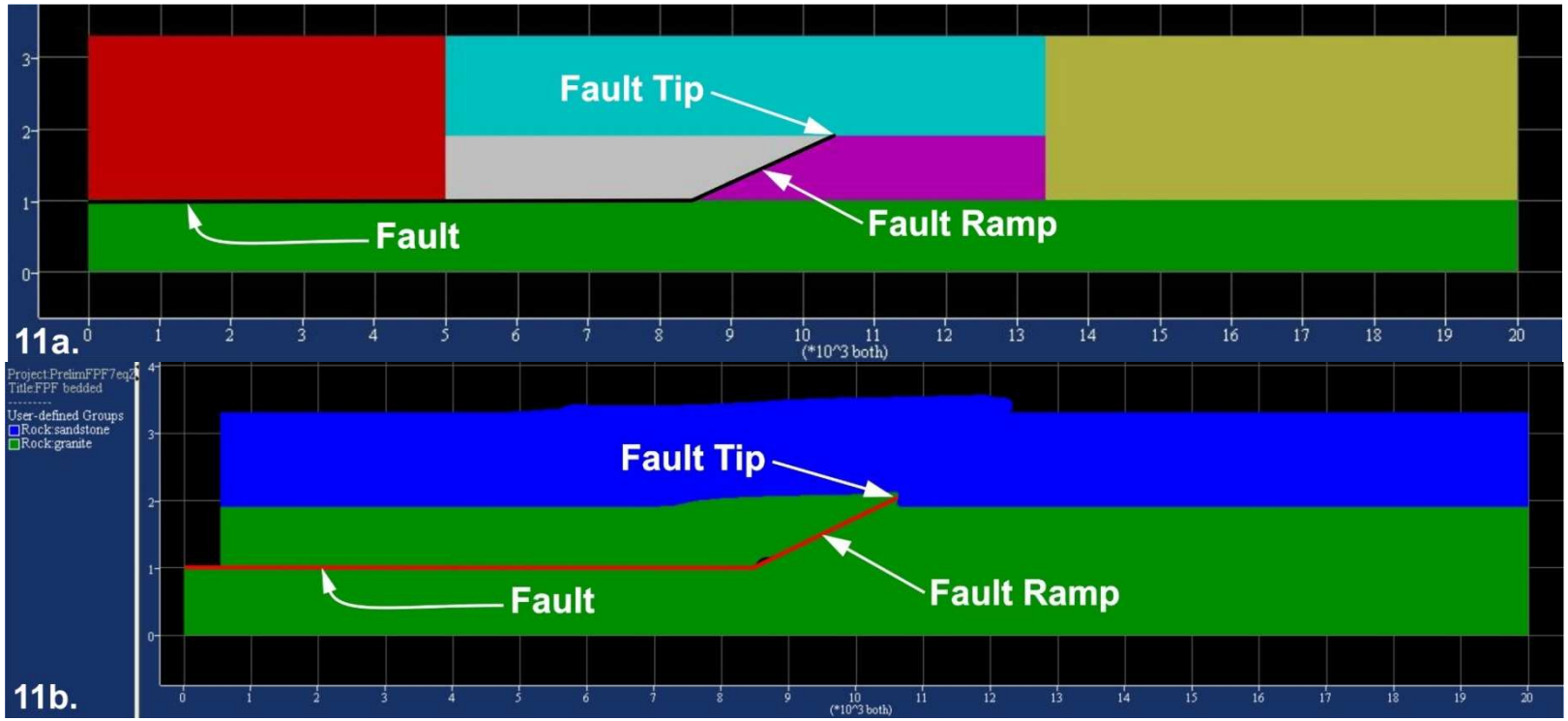

Figure B.27: Initial position - 11a and final - 11b; granite and sandstone above fault. Scale of axes – 1 km.

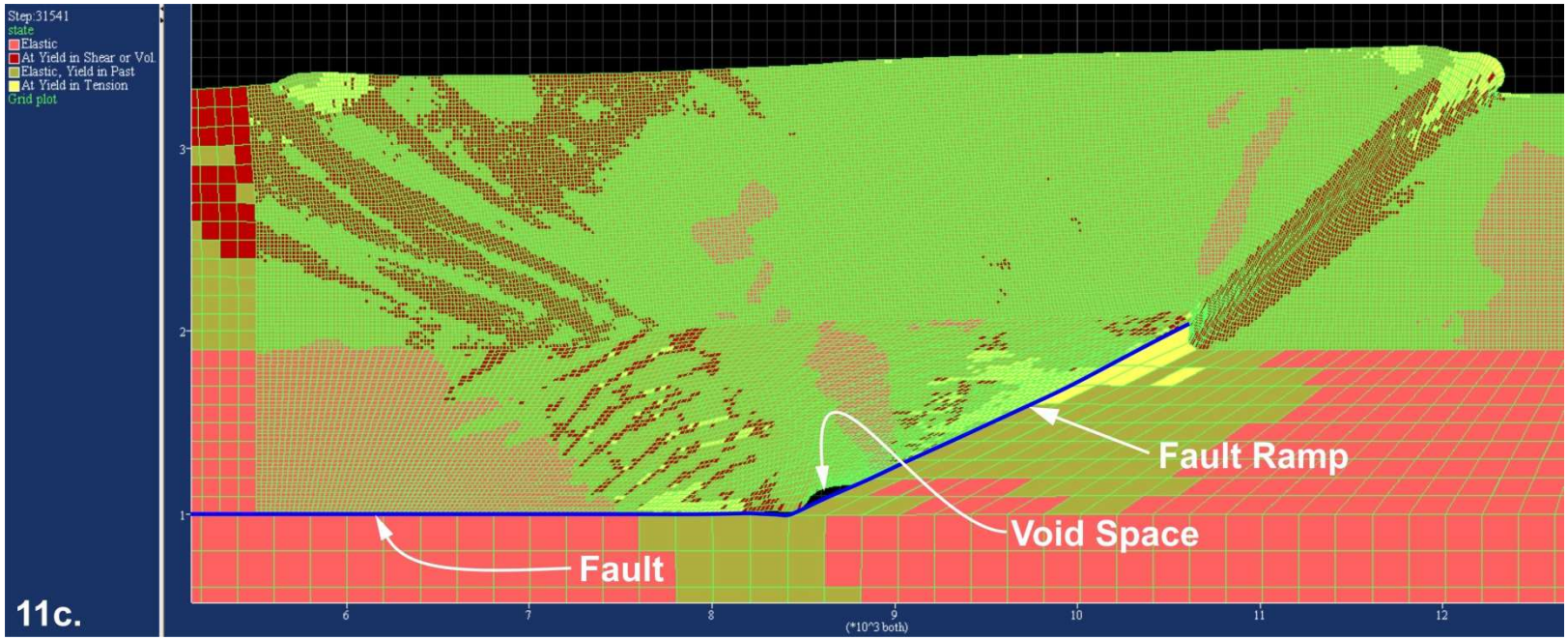

Figure B.28: Backthrust shear bands, model 11; granite and sandstone above fault. Shear bands are wider. Scale of axes – 1 km.

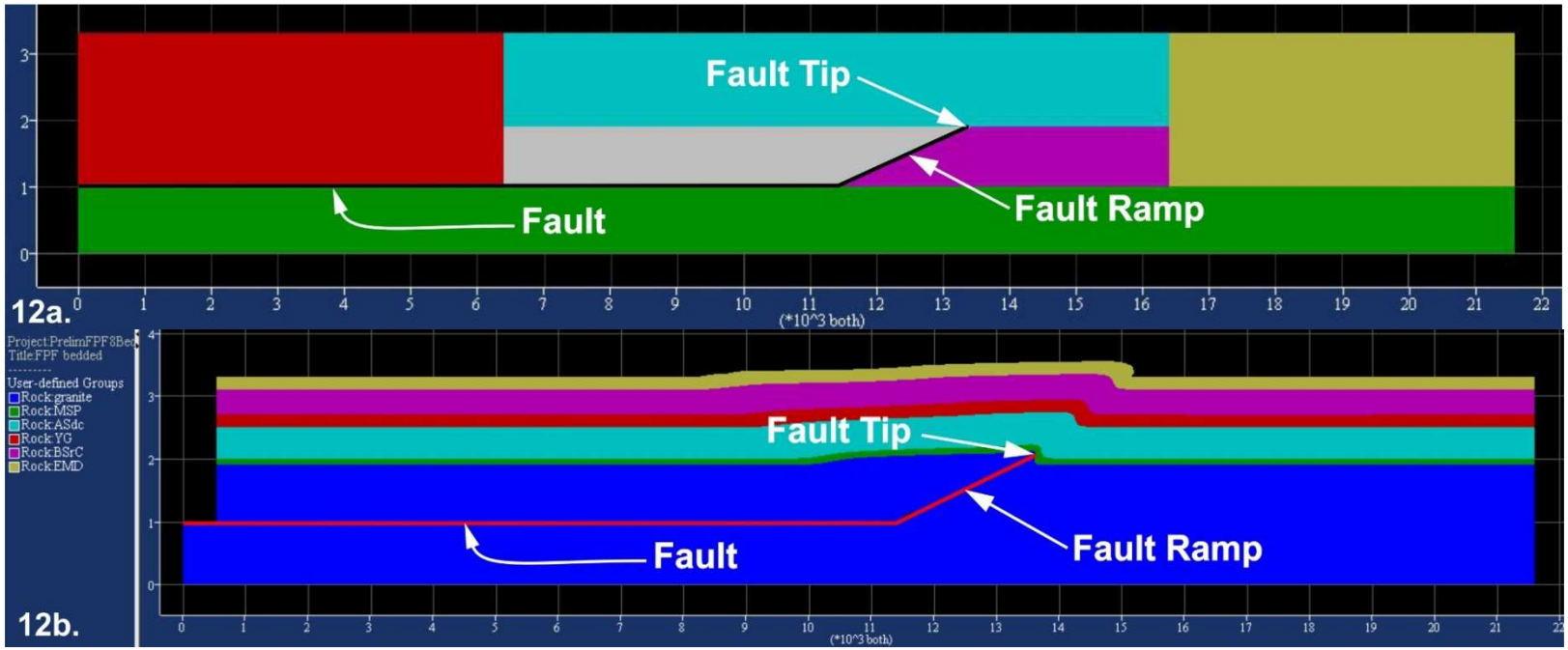

Figure B.29: Initial position - 12a and final - 12b; strata of study area. Scale of axes – 1 km.

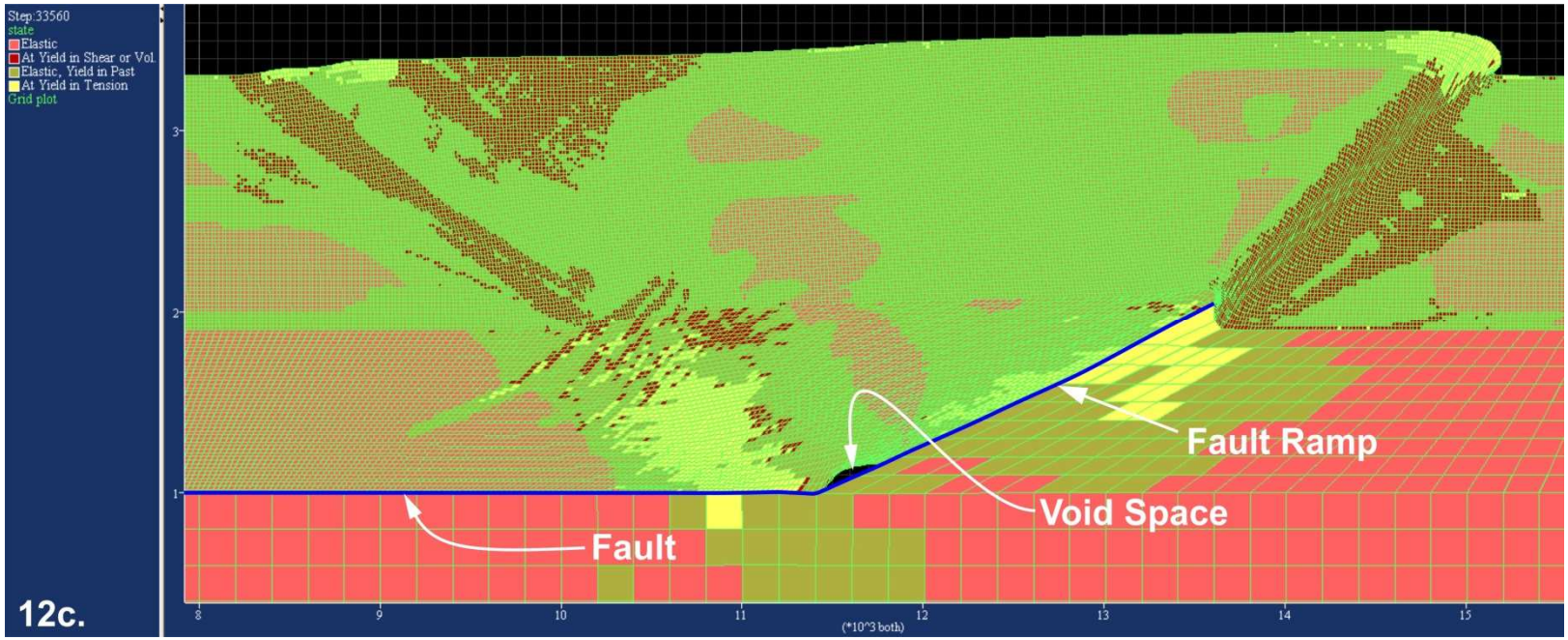

Figure B.30: Backthrust shear bands, model 12; strata of study area above fault. Shear bands are wider. Scale of axes – 1 km.

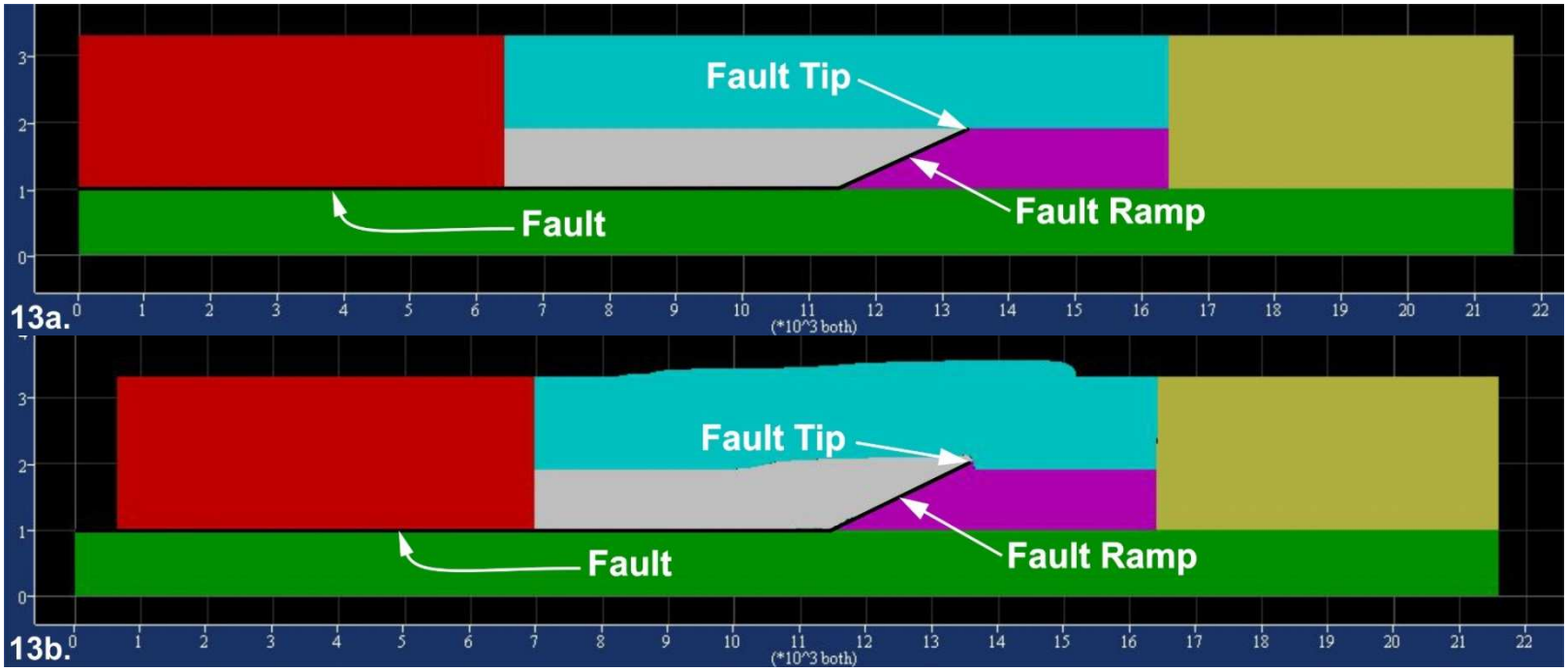

Figure B.31: Initial position - 13a and final - 13b; strata of study area. Scale of axes 1 km.

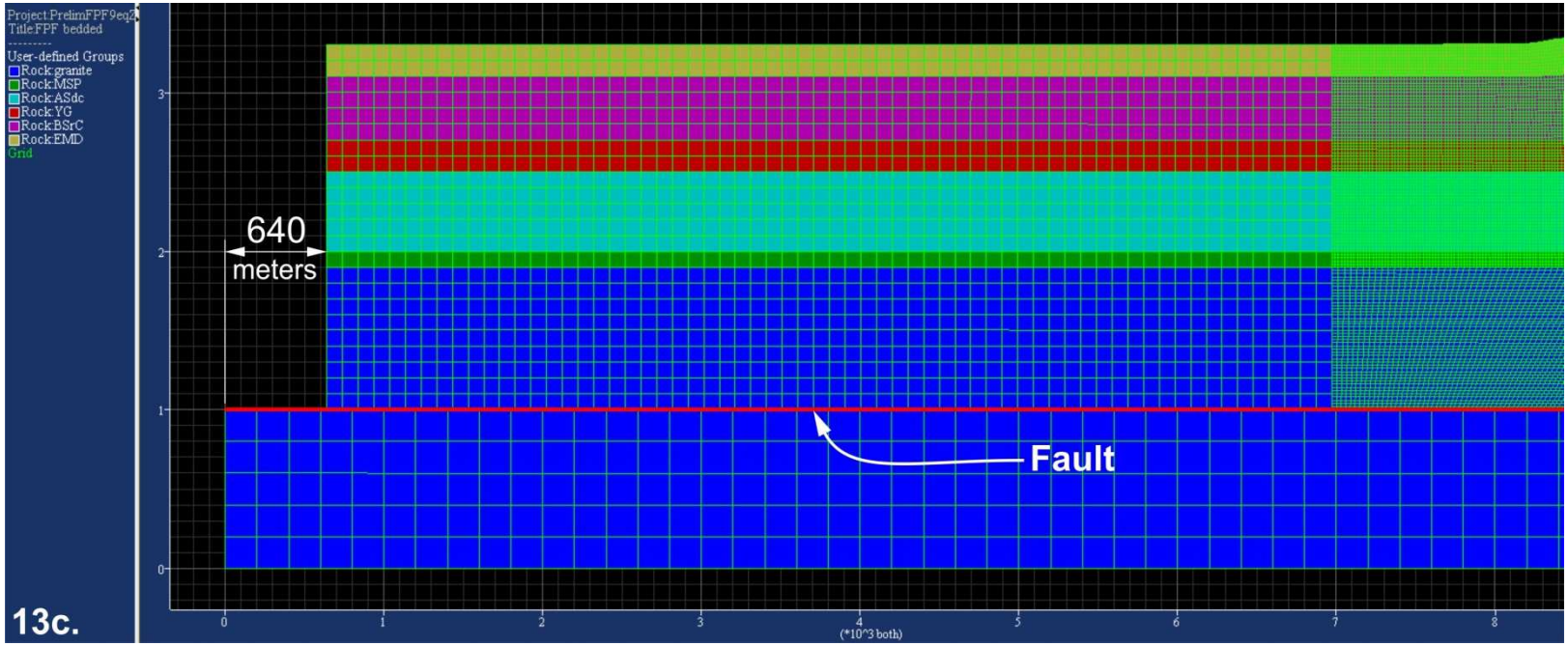

Figure B.32: Model 13 displacement at left-hand end. Scale of axes – 1 km.

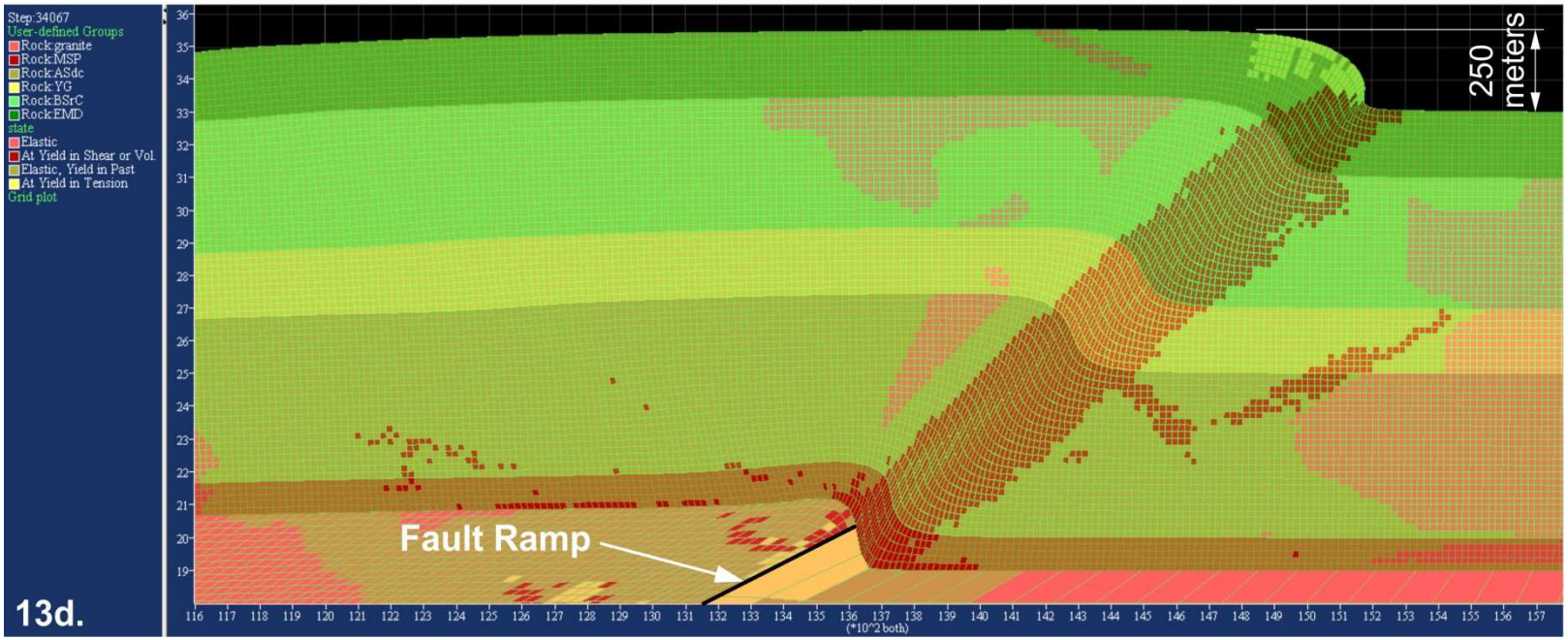

Figure B.33: Model 13 fault tip close up of shear bands. Scale of axes – 100 m.

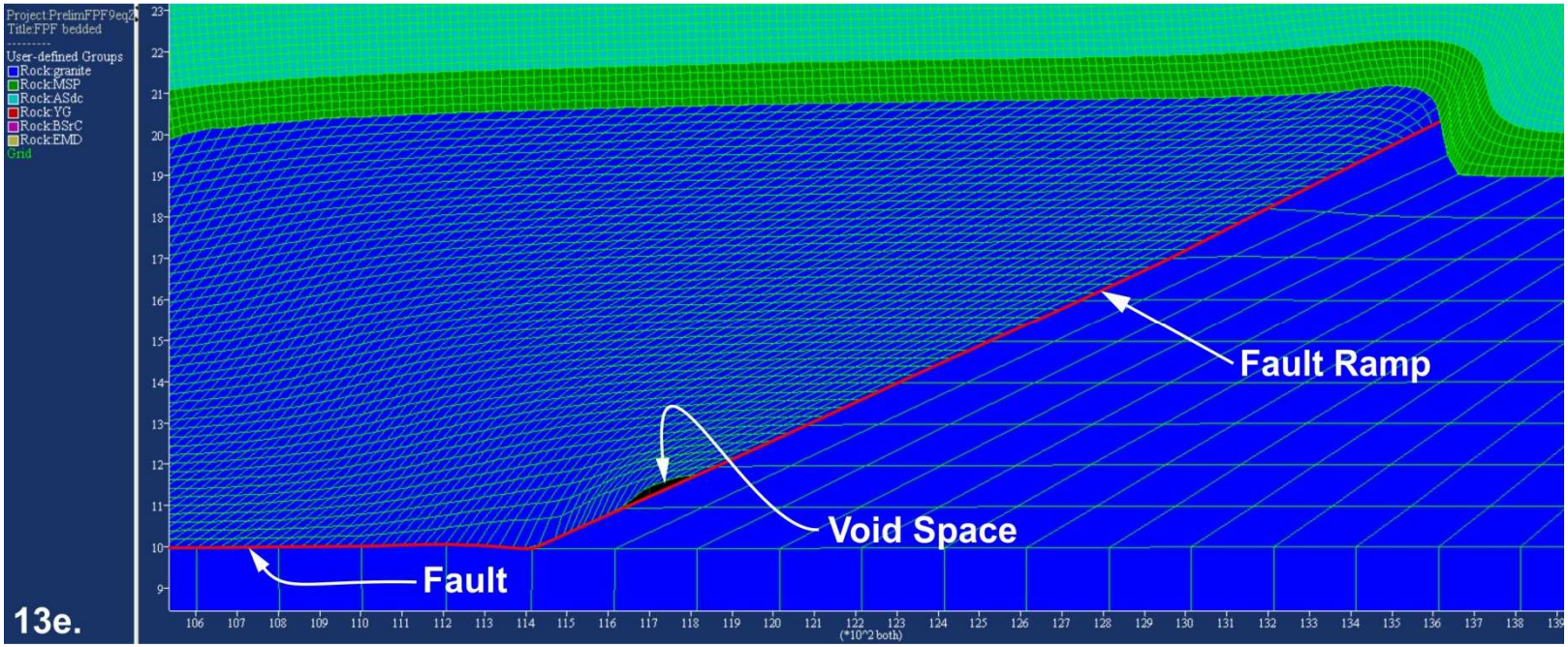

Figure B.34: Model 13 close up of void space at fault ramp. Scale of axes 100 m.

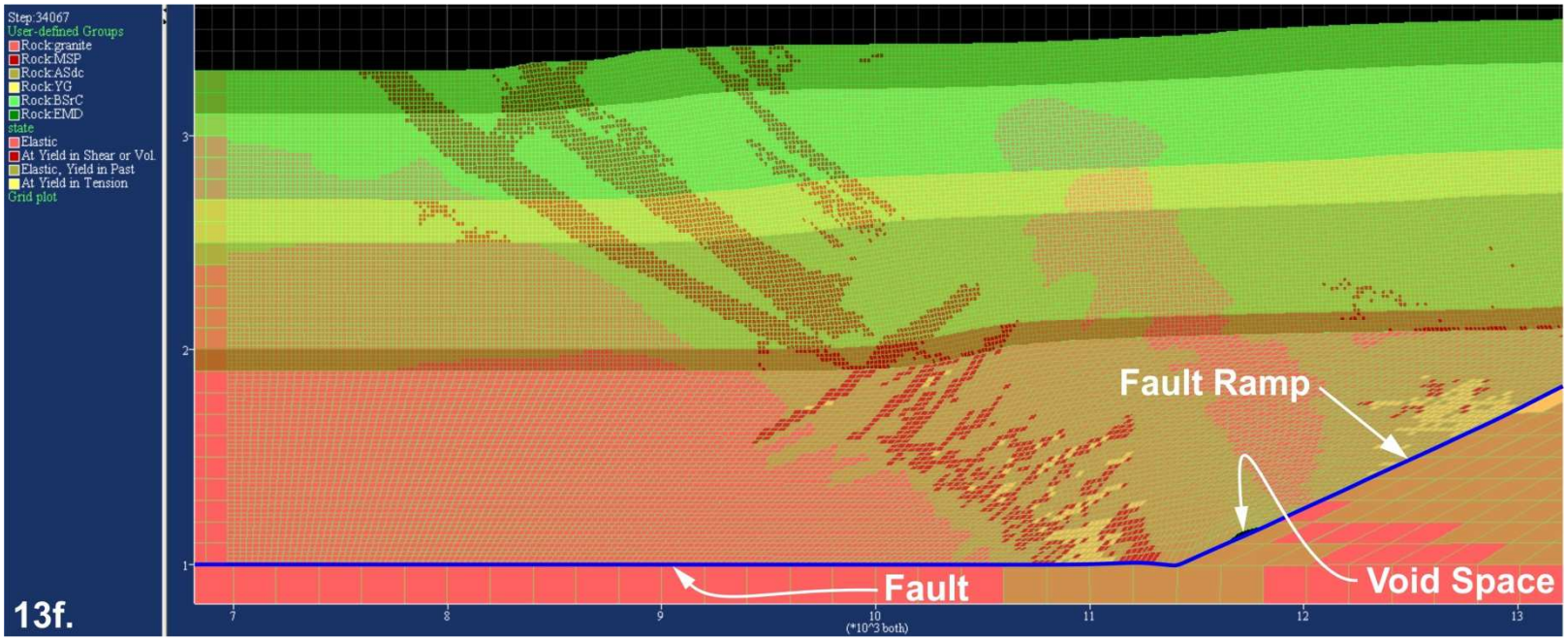

Figure B.35: Backthrust shear bands, model 13; strata of study area above fault. Shear bands are wider. Scale of axes – 1 km.

References

Baltz, E.H., 1972, Geologic Map and Cross Sections of the Gallinas Creek Area, Sangre De Cristo Mountains, San Miguel County, New Mexico: Miscellaneous Geologic Investigations, Map I-673, scale 1:24,000, 2 sheets.

Cardozo, N., and Cuisiat, F., 2008, Fault propagation folding modeling in FLAC, *in* Proceedings, 1st International *FLAC/DEM* Symposium, Minneapolis, Minnesota, August 25-27, Continuum and Distinct Element Numerical Modeling in Geo-Engineering - Hart, DeTournay & Cundall (eds.), Paper: 05-04, Itasca Consulting Group, Inc., Minneapolis, MN, USA.

Coetzee, M.J., Hart, R.D., Varona, P.M., and Cundall, P.A., 1993, ***FLAC* Basics** *An Introduction to FLAC and a guide to its practical application in geotechnical engineering,* Itasca Consulting Group, Inc., Minneapolis, Minnesota, 68 p.

Erickson, S.G., Strayer, L.M., and Suppe, J., 2001, Initiation and reactivation of faults during movement over a thrust-fault ramp: numerical mechanical models: Journal of Structural Geology, v. 23, p. 11-23, doi: 10.1016/S0191-8141(00)00074-2.

Gerbault, M., Poliakov, A.N.B., and Daignieres, M., 1998, Prediction of faulting from the theories of elasticity and plasticity: what are the limits?: Journal of Structural Geology, v. 20, No. 2/3,p. 301-320, doi: 10.1016/S0191-8141(97)00089-8.

Harper, T.R., 2008, Numerical experiments to investigate faulting and the dynamics of tectonic processes, *in* Proceedings, 1st International *FLAC/DEM* Symposium, Minneapolis, Minnesota, August 25-27, Continuum and Distinct Element Numerical Modeling in Geo-Engineering - Hart, DeTournay & Cundall (eds.), Paper: 05-01, Itasca Consulting Group, Inc., Minneapolis, MN, USA.

Itasca Consulting Group, Inc., 2002, ***FLAC****-Fast Lagrangian Analysis of Continua, Ver. 4.0 User's Manual*, Itasca Consulting Group, Inc., Minneapolis, MN, USA.

Jing, L., 2003, A review of techniques, advances and outstanding issues in numerical modelling for rock mechanics and rock engineering: International Journal of Rock Mechanics and Mining Sciences, v. 40, p. 283-353, doi: 10.1016/S1365-1609(03)00013-3.

Jing, L., and Hudson, J.A., 2002, Numerical methods in rock mechanics: International Journal of Rock Mechanics and Mining Sciences, v. 39, p. 409-427, doi: 10.1016/S1365-1609(02)00065-5.

Nino, F., Philip, H., and Chery, J., 1998, The role of bed-parallel slip in the formation of blind thrust faults: Journal of Structural Geology, v. 20, No. 5, p. 503-516, doi: 10.1016/S0191-8141(97)00102-8.

Poliakov, A.N.B., and Herrmann, H.J., 1994, Self-organized criticality of plastic shear bands in rocks: Geophysical Research Letters, v. 21, No. 19, p. 2143-2146, doi: 10.1029/94GL02005.

Smart, K.J., Ferrill, D.A., and Morris, A.P., 2009, Impact of interlayer slip on fracture prediction from geomechanical models of fault-related folds: AAPG Bulletin, v. 93, no. 11 (November), p. 1447-1458.

Starfield, A.M., and Cundall, P.A., 1988, Towards a Methodology for Rock Mechanics Modeling: International Journal of Rock Mechanics and Mining Sciences & Geomechanics, Abstracts, v. 25, No. 3, p. 99-106, doi: 10.1016/0148-9062(88)92292-9.

Strayer, L.M., and Hudleston, P.J., 1997, Numerical modeling of fold initiation at thrust ramps: Journal of Structural Geology, v. 19, Nos. 3-4, p. 551-566, doi: 10.1016/S0191-8141(96)00109-5.

Vermeer, P.A., and de Borst, R., 1984, Non-associated plasticity for soils, concrete and rock: Heron, v. 29, no. 3, p. 1-64.

Whittaker, B.N., Singh, R.N., and Sun, G., July 1992, Rock Fracture Mechanics: Principles, Design and Applications (Developments in Geotechnical Engineering): Elsevier Science Ltd, p. 349-371.

Biographical Information

Jerry Timothy Ford, known as Tim by his family and friends, was first inspired to study geology by Dr. John Wickham during a field lab exercise to Oklahoma. All of his life, he has enjoyed the outdoors, but had never considered the study of geology as being exciting and fulfilling until meeting Dr. Wickham. He now enjoys going on rock hunting trips with his family, who all happen to be true “rock hounds”. He looks forward in pursuing a career to further his knowledge in geology, especially the structure and the rocks formed from those structures.